Fig. 4. NOESY correlations of the trimethyloxabicyclo[2.2.1]heptane unit of 1.

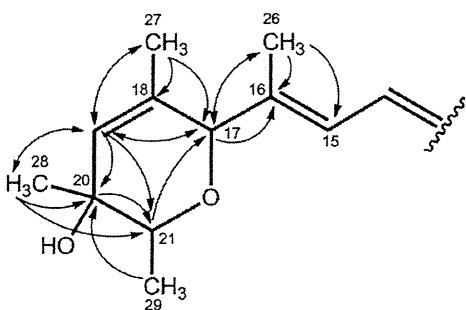Fig. 5. HMBC correlations of the dihydropyran unit of 1.

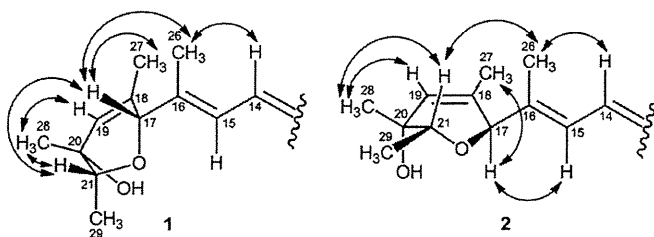Fig. 6. NOESY correlations of the dihydropyran unit of 1 and 2.

complexes I, III, and IV) and succinate-cytochrome c reductase (constituted of complexes II and III) from bovine heart was weak, with IC$_{50}$ values of 9000 nM and 68,000 nM, respectively. Next we examined the selectivity of inhibitory activity of 1 against each complex. Compound 1 inhibited NADH-rhodoquinone reductase (complex I) activity with an IC$_{50}$ value of 55 nM, but it did not affect rhodoquinol-fumarate reductase (complex II) activity at 100 µM. On the other hand, 1 showed only weak inhibitory activities against each complex of bovine heart. Therefore 1 is concluded to be a selective inhibitor of helminth complex I, similar to nafuredin.[2a]

Table 2
Inhibition of electron transport enzymes by 1 and 2

	Enzyme	Complex	IC$_{50}$ (nM)	
			1	2
A. suum	NADH-fumarate reductase	I+II	2.4	470
	NADH-rhodoquinone reductase	I	55	NT
	Rhodoquinol-fumarate reductase	II	>100,000	NT
Bovine heart	NADH oxidase	I+III+IV	9000	16,000
	Succinate-cytochrome c reductase	II+III	68,000	30,000
	NADH-ubiquinone reductase	I	28,000	NT
	Succinate-ubiquinone reductase	II	>100,000	NT
	Ubiquinol-cytochrome c reductase	III	32,000	NT

NT: not tested.

The IC$_{50}$ value of the epimer 2 against NFRD was 470 nM, about 200 times weaker than 1. However 2 inhibited NADH oxidase and succinate-cytochrome c reductase at the IC$_{50}$ values of 16,000 nM and 30,000 nM, respectively, which were similar to those of 1. These data suggested 1 had more helminth specific-NFRD inhibitory activity compared to 2. The specificity might be due to the conformation of the dihydropyran ring, which would be considerably changed by altering the configuration of C-17.

Furthermore, we obtained prugosene A1 from culture broth of another fungus Penicillium sp. FKI-5329, and measured the NFRD inhibitory activity.[11] The IC$_{50}$ values of prugosene A1 against NFRD and NADH oxidase were 13 nM and 8600 nM, respectively, similar to those of 1. The data suggested that the (17S)-epimer was more potent inhibitor and the conformation of dihydropyran ring was much more important than 2-oxabicyclo[2.2.1]heptane unit for Ascaris enzyme-specific inhibition. In addition, the results indicated the methyl moiety at C-8 did not affect the inhibitory activity.

We evaluated the cytotoxicity of 1 using human T-lymphocyte Jurkat cells by MTT method.[12] Morphological change and growth inhibition were observed by 1 at high concentration. The IC$_{50}$ value of growth inhibition was 21 µM, about 8800 times weaker than that of NFRD inhibition (2.4 nM). Antimicrobial activities of 1 were tested by an agar dilution method.[13] As well as prugosenes,[8] 1 did not show antimicrobial activities against Gram-positive and Gram-negative bacteria and fungi at 100 µg/mL (214 µM). Therefore, 1 and prugosene A1 are expected to be selective and potent NFRD inhibitors.

NMR spectra of 1, the chemical shifts of signals assigned to the dihydropyran ring were changed from 1 (Table 1), although the HMBC correlations showed 1 and 2 had the same planar structure. These results suggested 2 had a different configuration in the dihydropyran ring moiety compared with 1. This was elucidated by a NOESY experiment. The NOEs observed in the dihydropyran ring of 2 are shown in Fig. 6. Compared with the data of 1, the NOE correlation between H-17 and H-21 is not observed and the correlation between H-15 and H-17 was only observed in 2. Therefore, the relative configuration was defined as (17R,20R,21R). We also confirmed the 2-oxabicyclo[2.2.1]heptane unit had the same configuration (2S,4R,5S,6S) as that of 1 by analysis of NOESY data. From the above data 2 was elucidated to be the C-17 epimer (17R-epimer) of 1. While the difference between two compounds was only the conformation of C-17, 2 was much more labile than 1.

3. Biological activities

Inhibitory activities of 1 and 2 against electron transport system enzymes were evaluated using submitochondrial particles of A. suum and bovine heart (Table 2). Compound 1 inhibited NADH-fumarate reductase (NFRD, composed of complexes I and II) from A. suum with an IC$_{50}$ value of 2.4 nM, although the inhibition against mammal enzymes NADH oxidase (constituted with

4. Experimental

4.1. General

UV spectra were measured by Hitachi UV/Vis spectrometer U-2810. Optical rotations were recorded by means of JASCO DIP-1000 polarimeter. FT-IR spectra were conducted on Horiba FT-170. NMR spectra were recorded on 300 MHz (Varian XL-300), 400 MHz (Varian XL-400), and 600 MHz (Varian Inova 600) NMR spectrometer. For calibration of ^{13}C and ^{1}H chemical shifts, the carbon signal and residual proton signal of CDCl$_3$ were used (CDCl$_3$: δ_H 7.26 ppm and δ_C 77.0 ppm). FABMS and HRFABMS spectra were measured on JEOL JMS-AX505HA. Normal phase HPLC analysis was

performed using Pegasil silica column (4.6φ×250 mm) applying CHCl₃/acetone (100:1). Reverse phase HPLC analysis was performed using Pegasil ODS column (4.6φ×250 mm) applying CH₃CN/H₂O (65:35). Adults *A. suum* and bovine heart were purchased from Tokyo Shibaura Zouki Co. Ltd.

4.2. Organisms

The fungus *Penicillium* sp. FKI-3389 was isolated from a soil sample collected in Hilo, Hawaii, USA. By the sequence data of ITS rDNA and morphological characteristics, the fungus FKI-3389 was identified to be a member of the *Penicillium* genus. The ITS sequence of the strain FKI-3389 was deposited at the DNA Data Bank of Japan with accession number AB455515. The fungus FKI-3389 was deposited at the NITE Patent Microorganisms Depositary, National Institute of Technology and Evaluation, Kisarazu, Chiba, Japan as NITE BP-244.

4.3. Fermentation

One loopful of the strain FKI-3389 grown on LcA slant (glycerol 0.1%, KH₂PO₄ 0.08%, K₂HPO₄ 0.02%, MgSO₄·7H₂O 0.02%, KCl 0.02%, NaNO₃ 0.2%, and agar 1.5%, pH 6.0) was inoculated into 500-mL Erlenmeyer flask containing 100 mL of a seed culture medium (glucose 2%, yeast extract 0.2%, MgSO₄·7H₂O 0.05%, polypeptone 0.5%, KH₂PO₄ 0.1%, and agar 0.1%, pH 6.0) and incubated on a rotary shaker at 27 °C for 2 days. A 1-mL of the seed culture was inoculated into each of sixty 500-mL Erlenmeyer flasks containing a production medium (50 g of water-sodden rice). Fermentation was carried out statically at 27 °C for 13 days.

4.4. Isolation

Moldy rice (3 kg) was extracted with 3.0 L of EtOAc. After the rice was removed by filtration the extract was concentrated in vacuo to afford a brown oil (14 g). The oil was applied to a silica gel column (48φ×450 mm) and washed with CHCl₃. Active materials eluted with CHCl₃/MeOH (100: 1) were concentrated to yield a crude material (2.7 g), which was then chromatographed over another silica gel column (30φ×330 mm). After washing with CHCl₃, the active materials were eluted with CHCl₃/MeOH (100:0 to 100:1). The active materials (1.9 g) were purified by preparative HPLC (column, Pegasil silica, 20φ×250 mm; mobile phase, CHCl₃/acetone (100:1); flow rate, 7.0 mL/min; detection, UV at 360 nm). Ukulactones A (**1**) and B (**2**) were eluted at 11 and 17.5 min, respectively. Each fraction was concentrated to dryness in vacuo to afford ukulactones A (**1**, 515 mg) and B (**2**, 3.5 mg) as yellow syrups.

4.4.1. Ukulactone A (1). Yellow syrup; $[\alpha]_D^{25}$ −54.0 (*c* 0.1, MeOH); UV (MeOH) λ_{max} (log ε) 243 (sh, 3.38), 308 (sh, 4.29), 325 (4.60), 340 (4.78), 358 (4.76) nm; IR ν_{max} (NaCl) 3730, 3595, 2927, 2858, 1795, 1745 cm⁻¹; HRFABMS *m/z* 466.2722 ([M]⁺, 466.2719 calcd for C₂₉H₃₈O₅); ¹H and ¹³C NMR, see Table 1.

4.4.2. Ukulactone B (2). Yellow syrup; $[\alpha]_D^{25}$ +87.5 (*c* 0.1, MeOH); UV (MeOH) λ_{max} (log ε) 245 (sh, 3.30), 309 (sh, 4.07), 325 (4.38), 340 (4.55), 359 (4.51) nm; IR ν_{max} (NaCl) 3730, 3593, 2922, 2856, 1797, 1743 cm⁻¹; HRFABMS *m/z* 466.2710 ([M]⁺, 466.2719 calcd for C₂₉H₃₈O₅); ¹H and ¹³C NMR, see Table 1.

4.5. Biological studies

4.5.1. Enzyme assays. NADH-fumarate reductase inhibitory activity was assayed using submitochondrial particles of *A. suum*. For the preparation of these particles containing NADH-fumarate reductase, muscle of *A. suum* (1 g) was homogenized in 3.5 mL of sodium phosphate buffer (120 mM, pH 7.0) and centrifuged at

1000×g for 10 min to remove cell debris. The supernatant was further centrifuged at 10,000×g for 30 min and the resultant mitochondrial precipitate was re-suspended in 3.5 mL of sodium phosphate buffer (120 mM, pH 7.0) before use.

NADH-fumarate reductase inhibitory activity was assayed by the following procedure; 80 μL of sodium phosphate buffer (120 mM, pH 7.0) containing 0.35 mM NADH and 7.2 mM disodium fumarate and 10 μL of DMSO/H₂O (1:1) solution of test compound were put into a 96-well plate and shaken for 3 min. The reaction was initiated by the addition of 10 μL of the submitochondrial fraction and the resultant mixture was incubated for 3 min at 37 °C. After incubation, absorbance at 340 nm was observed every 15 s for 10 min at 37 °C. The inhibitory activity was calculated as followed.

$$\text{Inhibition(\%)} = \left\{ 1 - \frac{\left(A_{slope}[\text{sample}] - A_{slope}[\text{no fumerate}]\right)}{\left(A_{slope}[\text{control}] - A_{slope}[\text{no fumerate}]\right)} \right\} \times 100$$

A: Absorbance at 340 nm.

NADH oxidase inhibitory activity and succinate-cytochrome *c* reductase inhibitory activity were assayed using submitochondrial particles of bovine heart. For preparation of submitochondrial particles from bovine heart muscles, chopped muscle (1 g) was homogenized in 5 mL of 120 mM sodium phosphate buffer (pH 7.0) and centrifuged at 1000×g for 10 min. The supernatant was further centrifuged at 10,000×g for 30 min and the resultant mitochondrial precipitate was re-suspended in 3.5 mL of sodium phosphate buffer (120 mM, pH 7.0). The suspension was centrifuged at 100,000×g for 30 min after ultrasonication and the submitochondrial particles were obtained as a precipitate. Before use, the precipitate was re-suspended in 3.5 mL of sodium phosphate buffer (120 mM, pH 7.0).

NADH oxidase inhibitory activity was assayed as follows: the phosphate buffer (80 μL) containing 0.70 mM NADH and 10 μL of DMSO/H₂O (1:1) solution of test compound were put into a 96-well plate and shaken for 3 min. The reaction was initiated by the addition of 10 μL of the submitochondrial fraction and the mixture was incubated for 3 min at 37 °C. After incubation, absorbance at 340 nm was observed every 15 s for 10 min at 37 °C. The inhibitory activity was calculated as followed.

$$\text{Inhibition(\%)} = \left\{ 1 - \frac{\left(A_{slope}[\text{sample}] - A_{slope}[\text{no enzyme}]\right)}{\left(A_{slope}[\text{control}] - A_{slope}[\text{no enzyme}]\right)} \right\} \times 100$$

A: Absorbance at 340 nm.

Succinate-cytochrome *c* reductase (SCRD) inhibitory activity was assayed by the following procedure: phosphate buffer (80 μL) containing 7.2 mM sodium succinate, 2.0 mg/mL of bovine cytochrome *c* and 1.3 mM potassium cyanide and 10 μL of DMSO/H₂O (1:1) solution of test compound were put into a 96-well plate and shaken for 3 min. The reaction was initiated by addition of 10 μL of the submitochondrial fraction and the mixture was incubated for 3 min at 37 °C. After incubation, absorbance at 550 nm was observed every 15 s for 10 min at 37 °C. The inhibitory activity was calculated as followed.

$$\text{Inhibition(\%)} = \left\{ 1 - \frac{\left(A_{slope}[\text{sample}] - A_{slope}[\text{no succinate}]\right)}{\left(A_{slope}[\text{control}] - A_{slope}[\text{no succinate}]\right)} \right\} \times 100$$

A: Absorbance at 550 nm.

Other enzyme activities were measured as described previously.[2a,14]

4.5.2. Cytotoxicity.

Methanol solutions of test compound were put into a 96-well plate and dried completely. Jurkat cells were plated on the sample plate at a density of 2×10^4 cells/well with 100 μL of culture medium. After 3 days cultivation at 37 °C with 5% CO_2, cell density and morphological changes in the cells were observed under a microscope. After observation, 10 μL of MTT solution (5 mg/mL MTT in PBS) was added to the cells and the plate was incubated at 37 °C with 5% CO_2 for 2 h. Then, 50 μL of MTT solvent (0.7 M SDS, 50% DMF, 2.5% 1 M HCl and 2% acetic acid in H_2O) was added to the cells. After 1 h incubation at 37 °C, absorbance at 550 nm was measured.

4.5.3. Antimicrobial assay.

Antimicrobial activity was measured using the agar dilution method, according to the method of the Japanese Society of Chemotherapy,[13] with the following strains: *Staphylococcus aureus* ATCC6538P, *Kocuria rhizophila* (*Micrococcus luteus*) ATCC9341, *Bacillus subtilis* ATCC6633, *Mycobacterium smegmatis* ATCC607, *Escherichia coli* NIHJ, *Salmonella typhimurium* KB20, *Pseudomonas aeruginosa* NBRC3080, *Xanthomonas oryzae* KB88, *Bacteroides fragilis* ATCC23745, *Morganella morganii* NBRC3168, *Proteus vulgaris* NBRC3167, *Acholeplasma laidlawii* Bm1 KB175, *Candida albicans* KF1, *Saccharomyces cerevisiae* ATCC9763, *Aspergillus niger* ATCC9642, *Pyricularia oryzae* KF180 and *Mucor racemosus* NBRC4581.

Acknowledgements

References and notes

1. (a) Kita, K.; Nihei, C.; Tomitsuka, E. *Curr. Med. Chem.* **2003**, *10*, 2535–2548; (b) Kita, K.; Shiomi, K.; Ōmura, S. *Trends Parasitol.* **2007**, *23*, 223–229; (c) Masuma, R.; Shiomi, K.; Ōmura, S. In *The Mycota*; Anke, T., Weber, D., Eds.; Springer: Berlin Heidelberg, 2009; Vol. XV, pp 247–271.
2. (a) Ōmura, S.; Miyadera, H.; Ui, H.; Shiomi, K.; Yamaguchi, Y.; Masuma, R.; Nagamitsu, T.; Takano, D.; Sunazuka, T.; Harder, A.; Kölbl, H.; Namikoshi, M.; Miyoshi, H.; Sakamoto, K.; Kita, K. *PNAS* **2001**, *98*, 60–62; (b) Ui, H.; Shiomi, K.; Yamaguchi, Y.; Masuma, R.; Nagamitsu, T.; Takano, D.; Sunazuka, T.; Namikoshi, M.; Ōmura, S. *J. Antibiot.* **2001**, *54*, 234–238.
3. Miyadera, H.; Shiomi, K.; Ui, H.; Yamaguchi, Y.; Masuma, R.; Tomoda, H.; Miyoshi, H.; Osanai, A.; Kita, K.; Ōmura, S. *PNAS* **2003**, *100*, 473–477.
4. Ui, H.; Shiomi, K.; Suzuki, H.; Hatano, H.; Morimoto, H.; Yamaguchi, Y.; Masuma, R.; Sunazuka, T.; Shimamura, H.; Sakamoto, K.; Kita, K.; Miyoshi, H.; Tomoda, H.; Ōmura, S. *J. Antibiot.* **2006**, *59*, 785–790.
5. Ui, H.; Shiomi, K.; Suzuki, H.; Hatano, H.; Morimoto, H.; Yamaguchi, Y.; Masuma, R.; Sakamoto, K.; Kita, K.; Miyoshi, H.; Tomoda, H.; Tanaka, H.; Ōmura, S. *J. Antibiot.* **2006**, *59*, 591–596.
6. (a) de Haan, J. W.; van de Ven, L. J. M. *Tetrahedron Lett.* **1971**, 3965–3968; (b) Crews, P.; Kho-Wiseman, E. *J. Org. Chem.* **1977**, *42*, 2812–2815.
7. (a) Wei, H.; Itoh, T.; Kinoshita, M.; Kotoku, N.; Aoki, S.; Kobayashi, M. *Tetrahedron* **2005**, *61*, 8054–8058; (b) Wei, H.; Itoh, T.; Kotoku, N.; Kobayashi, M. *Heterocycles* **2006**, *68*, 111–123.
8. Lang, G.; Wiese, J.; Schmaljohann, R.; Imhoff, J. F. *Tetrahedron* **2007**, *63*, 11844–11849.
9. Jayasuriya, H.; Guan, Z.; Dombrowski, A. W.; Bills, G. F.; Polishook, J. D.; Jenkins, R. G.; Koch, L.; Crumly, T.; Tamas, T.; Dubois, M.; Misura, A.; Darkin-Rattray, S. J.; Gregory, L.; Singh, S. B. *J. Nat. Prod.* **2007**, *70*, 1364–1367.
10. Dong, Y.; Lin, J.; Lu, X.; Zheng, Z.; Ren, X.; Zhang, H.; He, J.; Yang, J. *Helv. Chim. Acta* **2009**, *92*, 567–574.
11. Prugosene A1 was isolated from molded rice with *Penicillium* sp. FKI-5329 by the same methods as shown in Experimental section. The structure of prugosene A1 was confirmed by the comparison with NMR data and FABMS spectrum.
12. Mosmann, T. *J. Immunol. Methods* **1983**, *65*, 55–63.
13. Nagayama, A.; Yamaguchi, K.; Watanabe, K.; Tanaka, M.; Kobayashi, I.; Nagasawa, Z. *J. Infect. Chemother.* **2008**, *14*, 383–392.
14. Saruta, F.; Kuramochi, T.; Nakamura, K.; Takamiya, S.; Yu, Y.; Aoki, T.; Sekimizu, K.; Kojima, S.; Kita, K. *J. Biol. Chem.* **1995**, *270*, 928–932.

Molecular interaction of the first 3 enzymes of the *de novo* pyrimidine biosynthetic pathway of *Trypanosoma cruzi*

Takeshi Nara [a,*], Muneaki Hashimoto [a], Hiroko Hirawake [a], Chien-Wei Liao [a,b], Yoshihisa Fukai [a], Shigeo Suzuki [a], Akiko Tsubouchi [a], Jorge Morales [a], Shinzaburo Takamiya [a], Tsutomu Fujimura [c], Hikari Taka [c], Reiko Mineki [c], Chia-Kwung Fan [b], Daniel Ken Inaoka [d], Masayuki Inoue [e], Akiko Tanaka [f], Shigeharu Harada [g], Kiyoshi Kita [d], Takashi Aoki [a]

[a] Department of Molecular and Cellular Parasitology, Juntendo University Graduate School of Medicine, 2-1-1 Hongo, Bunkyo-ku, Tokyo 113-8421, Japan
[b] Department of Parasitology, Taipei Medical University, 250 Wu-Xing Street, Taipei 110, Taiwan, ROC
[c] Division of Proteomics and Biomolecular Science, Biomedical Research Center, Juntendo University Graduate School of Medicine, 2-1-1 Hongo, Bunkyo-ku, Tokyo 113-8421, Japan
[d] Department of Biomedical Chemistry, Graduate School of Medicine, The University of Tokyo, 7-3-1 Hongo, Bunkyo-ku, Tokyo 113-0033, Japan
[e] Graduate School of Pharmaceutical Sciences, The University of Tokyo, 7-3-1 Hongo, Bunkyo-ku, Tokyo 113-0033, Japan
[f] Systems and Structural Biology Center, RIKEN, Tsurumi, Yokohama 230-0045, Japan
[g] Department of Applied Biology, Graduate School of Science and Technology, Kyoto Institute of Technology, Sakyo-ku, Kyoto 606-8585, Japan

ARTICLE INFO

ABSTRACT

The first 3 reaction steps of the *de novo* pyrimidine biosynthetic pathway are catalyzed by carbamoyl-phosphate synthetase II (CPSII), aspartate transcarbamoylase (ATC), and dihydroorotase (DHO), respectively. In eukaryotes, these enzymes are structurally classified into 2 types: (1) a CPSII-DHO-ATC fusion enzyme (CAD) found in animals, fungi, and amoebozoa, and (2) stand-alone enzymes found in plants and the protist groups. In the present study, we demonstrate direct intermolecular interactions between CPSII, ATC, and DHO of the parasitic protist *Trypanosoma cruzi*, which is the causative agent of Chagas disease. The 3 enzymes were expressed in a bacterial expression system and their interactions were examined. Immunoprecipitation using an antibody specific for each enzyme coupled with Western blotting-based detection using antibodies for the counterpart enzymes showed co-precipitation of all 3 enzymes. From an evolutionary viewpoint, the formation of a functional tri-enzyme complex may have preceded—and led to—gene fusion to produce the CAD protein. This is the first report to demonstrate the structural basis of these 3 enzymes as a model of CAD. Moreover, in conjunction with the essentiality of *de novo* pyrimidine biosynthesis in the parasite, our findings provide a rationale for new strategies for developing drugs for Chagas disease, which target the intermolecular interactions of these 3 enzymes.

© 2012 Elsevier Inc. All rights reserved.

1. Introduction

The *de novo* pyrimidine biosynthetic pathway consists of 6 enzymes required for the production of uridine 5'-monophosphate (UMP). In eukaryotes, the primary structure of the first 3 enzymes in this pathway, carbamoyl-phosphate synthetase II (CPSII; EC 6.3.5.5), aspartate transcarbamoylase (ATC; EC 2.1.3.2), and dihydroorotase (DHO; EC 3.5.2.3), is divided into 2 types [1]. A fusion enzyme of CPSII-DHO-ATC (CAD) is found in animals, fungi, amoebozoa, and also in the red alga *Cyanidioschyzon merolae* [2,3]. In contrast, the individual, stand-alone enzymes are common among the remaining eukaryotic groups.

Gene fusion results in the formation of multifunctional proteins and is one of the major driving forces in protein evolution. CAD has arisen from an ancient fusion between its monofunctional counterparts, which may result in enhanced channeling of substrates through each catalytic site [4]. From a biochemical viewpoint, it is assumed that formation of a complex of the enzymes preceded gene fusion and contributed to the precise order and topology of the domains within the fused enzyme. Moreover, ATC and DHO constitute an enzyme complex in a subset of bacteria [5,6], suggesting possible complex formation between eukaryotic ATC and DHO. Thus, it is highly likely that a tri-enzyme complex of stand-alone CPSII, ATC, and DHO preceded—and eventually led to—gene fusion to produce the multifunctional CAD protein, which may share tertiary structural similarity.

We have previously showed that CPSII, ATC, and DHO are stand-alone enzymes in the parasitic protist *Trypanosoma cruzi*, which is the causative agent of Chagas disease, an endemic disease in the Latin American countries [7,8]. All 5 genes for the 6 pyrimidine bio-synthetic enzymes cluster within trypanosomatid genomes in the following order: *CPSII, DHO, OMPDC-OPRT* (fused gene comprising the sixth orotidine-5′-monophosphate decarboxylase and the fifth orotate phosphoribosyltransferase enzymes), *DHOD* (the fourth dihydroorotate dehydrogenase enzyme), and *ATC*. Thus, the gene order of *CPSII, DHO*, and *ATC* in trypanosomatid genomes is consistent with the domain order within CAD [7]. Thus, these findings allowed us to investigate the possibility of complex formation between *T. cruzi* CPSII, ATC, and DHO.

From a clinical viewpoint, *de novo* pyrimidine biosynthesis represents a promising drug target, in particular, against Chagas disease and other trypanosomatid diseases such as sleeping sickness and leishmaniasis caused by *Trypanosoma brucei gambiense/rhodesiense* and *Leishmania* spp., respectively. These trypanosomatid diseases are termed "neglected tropical diseases", and urgently require effective chemotherapeutics with low toxicity [9,10]. Very recently, we demonstrated the importance of CPSII for the growth of *T. cruzi* in the cytoplasm of the mammalian host cells [11]. Therefore, the 3 enzymes and their complex, if present, represent potential targets of chemotherapy for trypanosomatid diseases.

In the present study, we used recombinant enzymes to examine whether CPSII, ATC, and DHO form a tertiary complex. As a result, we demonstrated that these 3 enzymes interact with each other, suggesting that the multifunctional CAD fusion enzyme was preceded by complex formation between CPSII, ATC, and DHO, possibly mimicking their tertiary structures. Thus, our findings provide important insights into the structural interpretation of evolution of enzymes as well as into the new strategic approaches for the development of drugs against Chagas disease.

2. Materials and methods

2.1. Plasmid construction

The open reading frames (ORFs) for the *T. cruzi CPSII* (GenBank ID: AB005063), *ATC* (GenBank ID: AB074139), and *DHO* (GenBank ID: AB010284) genes were subcloned into expression vectors, pET52b (ampicillin-resistant; Novagen, Merck Ltd., Tokyo, Japan), pET28a (kanamycin-resistant; Novagen), and pT-GroE (chloram-phenicol-resistant) [12]. Prior to cloning, pET52b was modified using the Gateway® Vector Conversion System (Invitrogen, Life Technologies Japan Ltd., Tokyo, Japan) by ligating a reading frame cassette A (RfA) to the *SmaI* site present in pET52b. The resulting plasmid was designated pET52bGW. For cloning of CPSII, the CPSII ORF was amplified using primers (sense, 5′-CACCATGTTTGGGG AAAAAGTGAA-3′; antisense, 5′- TCAACACTGAACGTCGCTGAAG GAGC-3′) and the phage clone carrying *CPSII*, subcloned into the pENTR vector (Invitrogen), and subsequently cloned into pET52bGW via the Clonase® reaction (Invitrogen). For expression of ATC, a pET14b plasmid carrying *ATC* [13] was digested with *BamHI* and the resulting DNA fragment was cloned into pET28a. For expression of DHO, the ORF was amplified by PCR using a primer set (sense, 5′-CACCATGACGCGGGTGGAACTGCC-3′ and antisense, 5′-CTAAATAGCCTTACCAACAAG-3′), subcloned into pENTR, and finally cloned into pET52bGW. Alternatively, the ORF of DHO was amplified using primers (sense, 5-′GCGAATTCCATATGA CGCG-3′; antisense, 5′-GCGGATCCTAAA-TAGCC-3′) and the phage clone carrying *DHO* [7] and subcloned into the pT7 BlueT vector. The *NdeI/BamHI* fragment was further subcloned into *NdeI/BamHI*-treated pT-GroE, in which the *GroESL* gene was cleaved off.

2.2. Expression of recombinant enzymes

Recombinant plasmids were introduced into *Escherichia coli* BL21 Star™ (DE3) cells (Invitrogen), either independently or in combination. The *E. coli* transformants were precultured by over-night incubation at 37 °C in Luria–Bertani (LB) medium containing the appropriate antibiotics. Subsequently, a total of 0.8 ml of the bacterial culture was centrifuged for 5 min at 1500g, and the cells were further cultured at 37 °C in 30 ml of antibiotic-supplemented LB medium until the OD_{600} reached 0.8. Expression was induced at 25 °C for 1 h in the presence of 0.4 mM isopropyl-β-D-thiogalacto-pyranoside. The cells were harvested by centrifugation at 1500g for 10 min and suspended in 2 ml of IP buffer (150 mM NaCl, 10 mM Tris–HCl [pH7.4], 1 mM EDTA, 1 mM EGTA, 1% Triton X-100, 1.5% NP-40, 0.2 mM sodium orthovanadate, and 0.2 mM PMSF) supplemented with a protease inhibitor cocktail (Complete Mini, Roche Diagnostics K.K., Tokyo, Japan). After disruption of cells by sonication, the lysate was centrifuged at 15,000g, 4 °C for 10 min. The resulting supernatant containing the soluble enzymes was collected and used for immunoprecipitation experiments.

2.3. Antibodies

Rabbit polyclonal IgG was raised against *T. cruzi* CPSII (polypep-tide, aa1–17; Sigma–Aldrich, St. Louis, MO) and DHO (polypeptide, aa12–29; BioGate Ltd, Gifu, Japan), and mouse polyclonal antisera was raised against recombinant *T. cruzi* ATC.

2.4. Immunoprecipitation

Immunoprecipitation was carried out using the enzyme-specific antibodies and Protein G Magnetic Beads (New England Biolabs, Beverly, MA) under the conditions recommended by the manufac-turer. Briefly, 200 μl of bacterial lysate was incubated at 4 °C for 1 h with 1.5 μg of purified IgG specific for each enzyme, followed by incubation with 25 μl of the beads at 4 °C for 1 h. The resulting pre-cipitates were recovered magnetically, separated by SDS–PAGE, and transferred to PVDF membranes. The membrane was reacted with enzyme-specific antibodies and visualized using alkaline phosphatase-conjugated secondary antibody and colorimetric substrates.

3. Results and discussion

The activities of CPSII, ATC, and DHO enzymes in trypanosomat-ids have been purified separately by gel chromatography or ammo-nium sulfate precipitation [14,15], suggesting that the 3 enzymes are not covalently linked, or that weak interactions occur between them. Thus, we aimed to examine the molecular interactions be-tween *T. cruzi* CPSII, ATC, and DHO by using purified enzymes that were independently expressed in a bacterial expression system (Fig. 1). *T. cruzi* ATC was efficiently expressed as a soluble protein and purified to apparent homogeneity, as reported previously [13]. However, individual expression of *T. cruzi* CPSII or DHO was difficult, and these enzymes were mainly expressed as insoluble inclusion bodies. The un-tagged recombinant *T. cruzi* DHO protein appeared to be toxic to *E. coli*, since the transformant colonies were very small (data not shown). This may be due to heterodimeriza-tion between bacterial and *T. cruzi* DHO proteins, thereby leading to impaired *de novo* pyrimidine biosynthesis by the bacteria. Fur-thermore, we also failed to obtain efficient expression of a soluble form of GST-tagged DHO.

Although these results suggest that individually expressed CPSII and DHO were highly unstable in the bacteria, we tried to examine
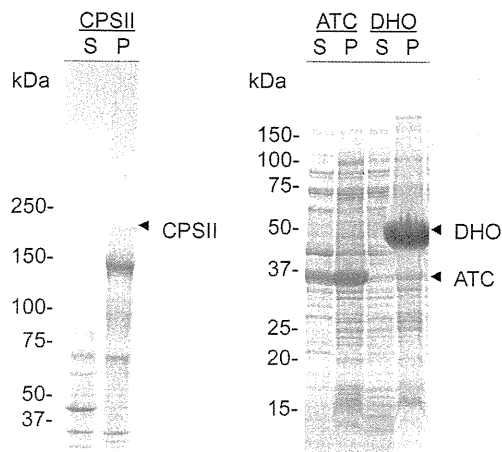
Fig. 1. Expression of the first 3 enzymes of the *Trypanosoma cruzi* de novo pyrimidine biosynthetic pathway in a bacterial expression system carbamoyl-phosphate synthetase II (CPSII), aspartate transcarbamoylase (ATC), and dihydro-orotase (DHO) were independently expressed in *E. coli* BL21 (DE3) Star cells, separated by SDS-PAGE, and stained with Coomasie Brilliant Blue. Recombinant CPSII and DHO were expressed mostly in the insoluble fractions (P), whereas ATC was expressed in both soluble (S) and insoluble fractions. The arrowheads indicate the respective protein bands.

whether the individually expressed enzymes formed a complex, which would stabilize these enzymes. The soluble fractions of each bacterial lysate were mixed, immunoprecipitated using the respective antibodies, and probed by Western blot analysis. However, no association was seen between the individually expressed target proteins.

Therefore, we examined the interactions between the 3 proteins by co-expressing CPSII, ATC, and DHO using pET52b (ampicillin-resistant), pET28a (kanamycin-resistant), and pT-GroE (chloram-phenicol-resistant) expression vectors, respectively, in order to confer antibiotic selection. Under these conditions, the trans-formed bacteria grew normally. After induction of expression, the bacterial lysates were immunoprecipitated using either CPSII- or ATC- or DHO-specific antibodies and subjected to Western blot analysis. As shown in Fig. 2, all 3 enzymes were co-precipitated
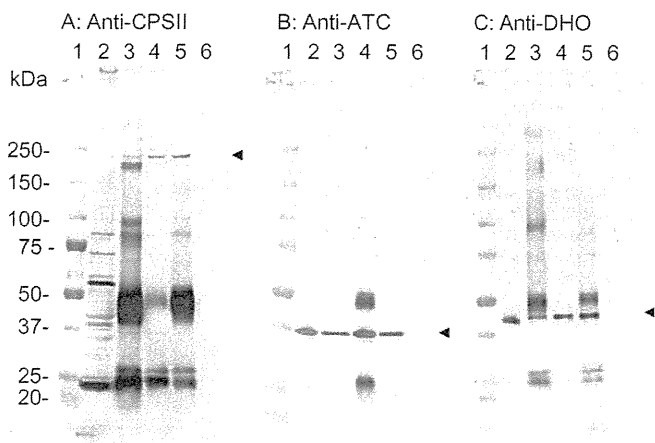

Fig. 2. Immunoprecipitation analysis of *E. coli* lysates co-expressing CPSII, ATC, and DHO. Western blot analysis was performed using antibodies specific to CPSII (panel A), ATC (panel B), and DHO (panel C). The *E. coli* lysates (lane 2) were immuno-precipitated using antibodies specific to CPSII (lane 3), ATC (lane 4), and DHO (lane 5), and examined by Western blotting. Precipitates using protein G beads in the absence of antibodies were loaded as a negative control (lane 6). An arrowhead indicates the respective target band. Lane 1, molecular weight marker.

by a pull-down assay using antibodies specific to either enzyme (Fig. 2). Namely, immunoprecipitation using the CPSII-specific antibody was accompanied by co-precipitation of both ATC and DHO, and the ATC- or DHO-specific antibodies allowed co-precipi-tation of CPSII plus DHO or CPSII plus ATC, respectively. Thus, these results clearly indicate the existence of a molecular interaction be-tween CPSII, ATC, and DHO.

Co-precipitation of ATC and DHO in the CPSII-specific precipi-tate was further confirmed by in-gel digestion coupled with liquid chromatography–tandem mass spectrometry (LC–MS/MS) of the corresponding protein bands separated by SDS–PAGE (Supplemen-tary Fig. S1). The sequence coverage scores for ATC and DHO were 52% and 51%, respectively. In addition, the ATC-specific precipitate was found to contain CPSII and DHO, and CPSII and ATC were de-tected in the DHO-specific precipitate (Supplementary Table S1). Therefore, these findings indicate complex formation by these non-covalently linked enzymes.

However, co-precipitation of CPSII with ATC and DHO does not necessarily indicate a direct interaction of CPSII with both ATC and DHO; if ATC interacts with DHO, the interaction of CPSII with either ATC or DHO would allow co-precipitation of all 3 enzymes. There-fore, we further examined the existence of a direct interaction of CPSII with ATC and DHO. CPSII was co-expressed with either ATC or DHO, and precipitated using the CPSII-specific antibody. Wes-tern blot analysis of the precipitates showed direct interactions be-tween both CPSII and ATC and between CPSII and DHO (Fig. 3). Similarly, a direct interaction was also observed between ATC and DHO, which is consistent with results for the bacterial en-zymes [5]. These findings strongly suggest that tri-enzyme com-plex formation between CPSII, ATC, and DHO occurs via direct interactions.

Regarding enzyme stability, native CPSII purified from the kine-toplastid *Crithidia fasciculata*—a close relative of trypanosomatids—was very fragile, and its enzyme activity was rapidly lost during cryopreservation, which may have been accompanied by dissocia-tion of its tertiary structure [16]. In the present study, the molecu-lar interactions between CPSII, ATC, and DHO were stable after repeated freezing and thawing. Therefore, it is possible that com-plex formation stabilizes enzyme conformation.

Recent advances in drug development have highlighted struc-ture-based drug design (SBDD) as a powerful tool. Moreover, inhib-itors of enzymes involved in *de novo* pyrimidine biosynthesis have been extensively studied because of the physiological importance of this pathway, particularly in rapidly growing cells such as cancer cells. However, SBDD has not yet been applied to CAD or its individual counterparts because of difficulties in their expression, purification, and crystallization and the resulting lack of structural information.

In the present study, we demonstrated for the first time the existence of a molecular interaction between *T. cruzi* CPSII, ATC, and DHO enzymes. Furthermore, the efficient expression of these proteins may aid structural analyses and the elucidation of a model of CAD, thereby leading to SBDD. Indeed, phylogenetic analysis has revealed that the trypanosomatid CPSII and ATC enzymes share common evolutionary origins with the corresponding domains in animal CAD [1].

Moreover, we recently identified the crystal structure of *T. cruzi* ATC [13]. This is the first crystallization of any of the 3 enzymes, including CAD proteins in eukaryotes. Therefore, our findings provide insight into SBDD targeted against trypanosomiasis, particularly aimed at inhibiting intermolecular interactions of the tri-enzymes. Although the phylogenetic relationship between *T. cruzi* DHO and the DHO domain of CAD remains unclarified, it is highly likely that the functional tri-enzyme complex of CPSII, ATC, and DHO occurred in the ancestral eukaryotes, thereby lead-ing to the formation of CAD via fusion of the 3 genes.
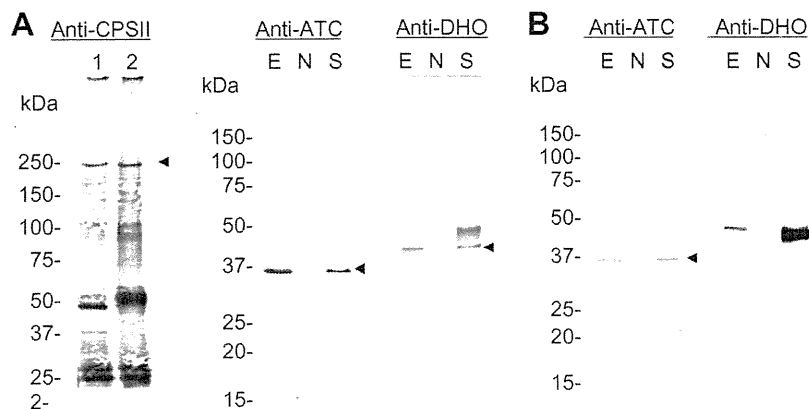
Fig. 3. Detection of the direct interactions between CPSII, ATC, and DHO In panel A, the bacterial lysates expressing CPSII together with ATC (lane 1) or DHO (lane 2) were immunoprecipitated using antibodies specific to the respective enzyme and probed using the CPSII-specific antibody (left). Alternatively, the bacterial extracts (E) expressing CPSII plus ATC or CPSII plus DHO were immunoprecipitated using the CPSII-specific antibody (S) and reacted with the antibody for ATC (middle) or DHO (right). In panel B, the bacterial extracts expressing ATC and DHO were immunoprecipitated using the antibody (S) for DHO (left) or ATC (right) and probed using the antibody for the counterpart enzymes. The immunoprecipitates in the absence of antibody (N) were loaded as a negative control. An arrowhead indicates the respective target band.

Since the *de novo* pyrimidine biosynthetic pathway is a potential primary target of chemotherapy [17,18], our findings may accelerate strategic approaches against trypanosomatid diseases based on SBDD that target the intermolecular interactions of the first 3 enzymes. Further analyses, including crystallography, are necessary to understand the molecular basis of the tri-enzyme complex.
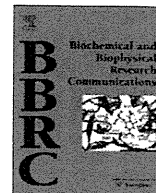
Acknowledgments

Appendix A. Supplementary data

Supplementary data associated with this article can be found, in the online version, at doi:10.1016/j.bbrc.2011.12.148.

References

[1] T. Nara, T. Hashimoto, T. Aoki, Evolutionary implications of the mosaic pyrimidine-biosynthetic pathway in eukaryotes, Gene 257 (2000) 209–222.

[2] M. Matsuzaki, O. Misumi, I.T. Shin, et al., Genome sequence of the ultrasmall unicellular red alga *Cyanidioschyzon merolae* 10D, Nature 428 (2004) 653–657.

[3] A. Stechmann, T. Cavalier-Smith, The root of the eukaryote tree pinpointed, Curr. Biol. 13 (2003) R665–666.

[4] E.A. Carrey, The shape of CAD, Paths to Pyrimidines 3 (1995) 68–72.

[5] P. Zhang, P.D. Martin, C. Purcarea, et al., Dihydroorotase from the hyperthermophile *Aquifex aeolicus* is activated by stoichiometric association with aspartate transcarbamoylase and forms a one-pot reactor for pyrimidine biosynthesis, Biochemistry 48 (2009) 766–778.

[6] M.J. Schurr, J.F. Vickrey, A.P. Kumar, et al., Aspartate transcarbamoylase genes of *Pseudomonas putida*: requirement for an inactive dihydroorotase for assembly into the dodecameric holoenzyme, J. Bacteriol. 177 (1995) 1751–1759.

[7] G. Gao, T. Nara, J. Nakajima-Shimada, et al., Novel organization and sequences of five genes encoding all six enzymes for de novo pyrimidine biosynthesis in *Trypanosoma cruzi*, J. Mol. Biol. 285 (1999) 149–161.

[8] T. Nara, G. Gao, H. Yamasaki, et al., Carbamoyl-phosphate synthetase II in kinetoplastids, Biochim. Biophys. Acta 1387 (1998) 462–468.

[9] R. Docampo, Recent developments in the chemotherapy of Chagas disease, Curr. Pharm. Des. 7 (2001) 1157–1164.

[10] J.A. Urbina, Chemotherapy of Chagas disease, Curr. Pharm. Des. 8 (2002) 287–295.

[11] M. Hashimoto, J. Morales, Y. Fukai, et al., Critical importance of the de novo pyrimidine biosynthesis pathway for *Trypanosoma cruzi* growth in the mammalian host cell cytoplasm, Biochem. Biophys. Res. Commun. (2012).

[12] T. Yasukawa, C. Kanei-Ishii, T. Maekawa, et al., Increase of solubility of foreign proteins in *Escherichia coli* by coproduction of the bacterial thioredoxin, J. Biol. Chem. 270 (1995) 25328–25331.

[13] K. Matoba, T. Nara, T. Aoki, et al., Crystallization and preliminary X-ray analysis of aspartate transcarbamoylase from the parasitic protist *Trypanosoma cruzi*, Acta Crystallogr. Sect. F Struct. Biol. Cryst. Commun. 65 (2009) 933–936.

[14] T. Aoki, H. Oya, Kinetic properties of carbamoyl-phosphate synthetase II (glutamine-hydrolyzing) in the parasitic protozoan *Crithidia fasciculata* and separation of the enzyme from aspartate carbamoyltransferase, Comp. Biochem. Physiol. B 87 (1987) 143–150.

[15] S. Tampitag, W.J. O'Sullivan, Enzymes of pyrimidine biosynthesis in *Crithidia luciliae*, Mol. Biochem. Parasitol. 19 (1986) 125–134.

[16] T. Aoki, H. Oya, Regulatory properties of carbamoyl-phosphate synthetase II from the parasitic protozoan *Crithidia fasciculata*, Comp. Biochem. Physiol. B 87 (1987) 655–658.

[17] J.A. Urbina, R. Docampo, Specific chemotherapy of Chagas disease: controversies and advances, Trends Parasitol. 19 (2003) 495–501.

[18] T. Annoura, T. Nara, T. Makiuchi, et al., The origin of dihydroorotate dehydrogenase genes of kinetoplastids, with special reference to their biological significance and adaptation to anaerobic, parasitic conditions, J. Mol. Evol. 60 (2005) 113–127.

Contents lists available at SciVerse ScienceDirect

Biochemical and Biophysical Research Communications

Critical importance of the *de novo* pyrimidine biosynthesis pathway for *Trypanosoma cruzi* growth in the mammalian host cell cytoplasm

Muneaki Hashimoto [a,*], Jorge Morales [a], Yoshihisa Fukai [a], Shigeo Suzuki [a], Shinzaburo Takamiya [a], Akiko Tsubouchi [a], Syou Inoue [a], Masayuki Inoue [b], Kiyoshi Kita [c], Shigeharu Harada [d], Akiko Tanaka [e], Takashi Aoki [a], Takeshi Nara [a,*]

[a] Department of Molecular and Cellular Parasitology, Juntendo University School of Medicine, 2-1-1 Hongo, Bunkyo-ku, Tokyo 113-8421, Japan
[b] Graduate School of Pharmaceutical Sciences, The University of Tokyo, 7-3-1 Hongo, Bunkyo-ku, Tokyo 113-0033, Japan
[c] Department of Biomedical Chemistry, Graduate School of Medicine, The University of Tokyo, 7-3-1 Hongo, Bunkyo-ku, Tokyo 113-0033, Japan
[d] Department of Applied Biology, Graduate School of Science and Technology, Kyoto Institute of Technology, Sakyo-ku, Kyoto 606-8585, Japan
[e] Systems and Structural Biology Center, RIKEN, Tsurumi, Yokohama 230-0045, Japan

ARTICLE INFO

ABSTRACT

The intracellular parasitic protist *Trypanosoma cruzi* is the causative agent of Chagas disease in Latin America. In general, pyrimidine nucleotides are supplied by both *de novo* biosynthesis and salvage pathways. While epimastigotes—an insect form—possess both activities, amastigotes—an intracellular replicating form of *T. cruzi*—are unable to mediate the uptake of pyrimidine. However, the requirement of *de novo* pyrimidine biosynthesis for parasite growth and survival has not yet been elucidated. Carbamoyl-phosphate synthetase II (CPSII) is the first and rate-limiting enzyme of the *de novo* biosynthetic pathway, and increased CPSII activity is associated with the rapid proliferation of tumor cells. In the present study, we showed that disruption of the *T. cruzi cpsII* gene significantly reduced parasite growth. In particular, the growth of amastigotes lacking the *cpsII* gene was severely suppressed. Thus, the *de novo* pyrimidine pathway is important for proliferation of *T. cruzi* in the host cell cytoplasm and represents a promising target for chemotherapy against Chagas disease.

© 2011 Elsevier Inc. All rights reserved.

1. Introduction

The parasitic protist *Trypanosoma cruzi* is the causative agent of Chagas disease [1]. The parasitic life cycle comprises 2 phases (the insect and mammalian stages) and includes three developmental forms—epimastigotes, trypomastigotes, and amastigotes [2]. Within the insect vector, the reduviid bug, epimastigotes replicate and transform into metacyclic trypomastigotes by a process termed metacyclogenesis. Non-proliferating metacyclic trypomastigotes invade the mammalian host and subsequently transform into amastigotes in a wide variety of nucleated cells. Intracellular amastigotes multiply by binary fission and then transform back into bloodstream trypomastigotes, which are released into the circulation after host cell disruption.

Pyrimidine is an essential component of nucleic acid structure. Thus, the biosynthesis of pyrimidine is a vital biological process,

which is achieved by both *de novo* synthesis and salvage pathways. Although both pathways have been shown to operate in *T. cruzi*, the parasite has only limited salvage activity. It has been reported that *T. cruzi* preferentially takes up more pyrimidine bases and nucleosides than nucleotides [3]. However, the host cell cytoplasm contains mainly nucleotides [4], which are not efficiently salvaged by *T. cruzi*. In addition, the intracellular amastigote lacks uracil phosphoribosyltransferase and uridine kinase enzymatic activities, the latter of which is not found in the *T. cruzi* genome [5]. Therefore, the *de novo* pyrimidine biosynthesis pathway may be important for *T. cruzi* growth in mammalian hosts.

The *de novo* pyrimidine biosynthetic pathway consists of a 6-enzyme cascade that catalyzes the formation of uridine 5′-monophosphate [6]. The first enzyme in the pathway is carbamoyl-phosphate synthetase II (CPSII, EC 6.3.5.5), which generates carbamoyl-phosphate from L-glutamine, bicarbonate, and two ATP molecules. Moreover, CPSII is a key regulatory enzyme of *de novo* pyrimidine biosynthesis, and increased CPSII activity is associated with the rapid proliferation of tumor cells [7].

In the present study, we established *T. cruzi* lacking the *CPSII* (*TcCPSII*) gene in order to determine the physiological relevance of *de novo* pyrimidine biosynthesis. By analyzing the mutant

parasites, we found that the *de novo* pyrimidine pathway is important for parasitic growth in the host cell.

2. Materials and methods

2.1. T. cruzi culture

T. cruzi epimastigotes (Tulahuen strain) were routinely subcultured on a weekly basis in liver infusion tryptose (LIT) medium (No. 1029, ATCC medium formulations) supplemented with 10% heat-inactivated fetal bovine serum (FBS) and 10 μg/ml hemin (Sigma–Aldrich, Japan) in tightly capped 25-cm^2 culture flasks at 27 °C. The mammalian stages of *T. cruzi* were maintained in HeLa cells, as previously described [8]. In addition, we used mouse embryonic fibroblast 3T3-Swiss ,albino cells (Health Science Research Resources Bank, Tokyo, Japan), which were maintained in Dulbecco's modified Eagle's medium (DMEM; Sigma–Aldrich Japan) supplemented with 10% FBS. For experiments, 3T3-Swiss cells were infected with metacyclic trypomastigotes at a multiplicity of infection (MOI) of 0.26. The infected cells were washed with PBS 24 h after infection to remove free parasites and cultured for a

further 3 days. Multiple infections of a single host cell by metacyclic trypomastigotes were confirmed as negligible under the experimental conditions employed. Infected *T. cruzi* amastigotes within host cells were stained with Diff-Quik solution (Sysmex, Kobe, Japan) and detected microscopically as previously described [8].

2.2. Metacyclogenesis

Metacyclogenesis was induced as previously described [9]. Epimastigotes from the late logarithmic phase were collected by centrifugation, suspended at a density of 1.0×10^7 cells/ml in 80% (v/v) RPMI-1640 medium and 20% (v/v) Grace's insect medium and incubated at 27 °C. Under these conditions, epimastigotes adhered to the surface of the plastic culture flask, and were released only once they enter metacyclogenesis [10]. For counting of metacyclic trypomastigotes, parasites that appeared in the culture supernatant were stained with Giemsa stain, and their morphology was evaluated by light microscopy according to the relative kinetoplast-nucleus position [10–12]. The efficacy of metacyclogenesis was evaluated by the ratio of epimastigotes to trypomastigotes in the culture supernatant 72 h after induction.
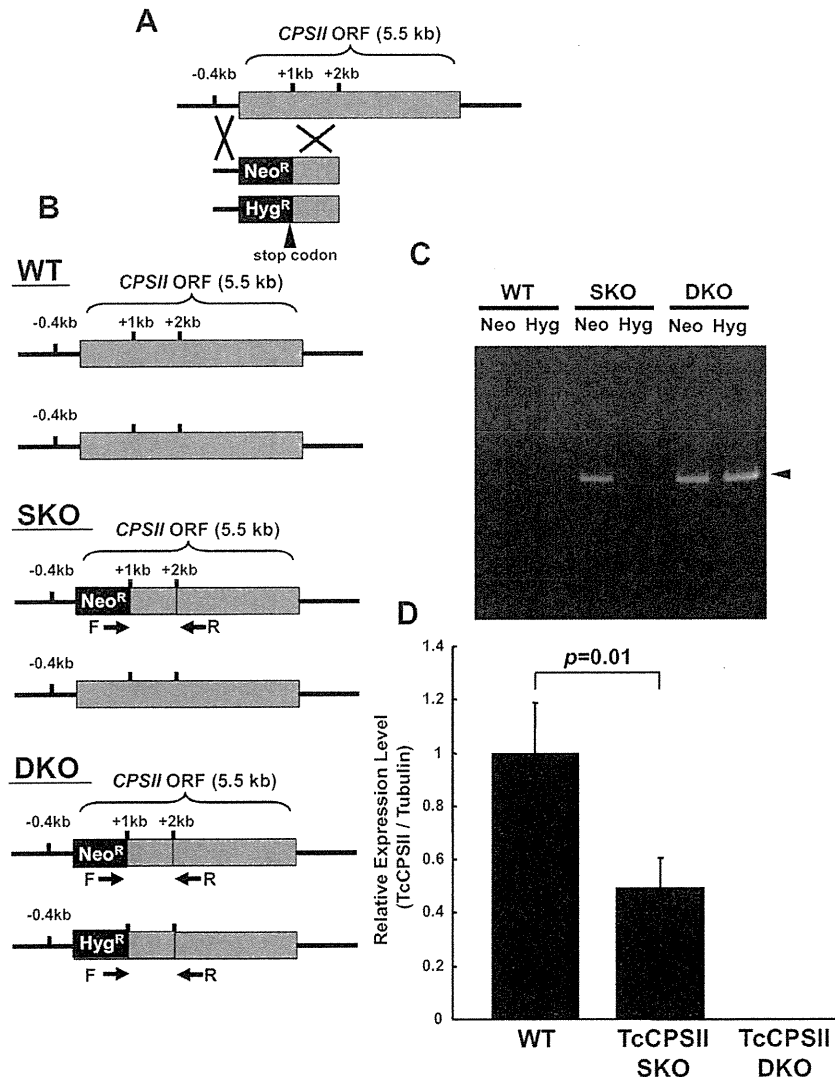

Fig. 1. Production of a *T. cruzi CPSII*-null mutant. (A) Diagram of the *TcCPSII* locus and neomycin- and hygromycin-resistance gene cassettes containing 5′-upstream (−0.41 kb) and 3′-downstream (+1.0 kb) sequences corresponding to the downstream region (+1 to +2 kb) of the *TcCPSII* open reading frame (ORF). (B) Schematic representation of *TcCPSII* loci in the WT, single-gene knockout (SKO), and double-gene knockout (DKO) parasites. (C) PCR analysis of genomic DNA from clones of the WT, SKO, and DKO parasites confirmed disruption of 1 locus of the *TcCPSII* gene in SKO parasites and disruption of the 2 loci in DKO parasites, respectively. (D) Real-time PCR analysis of *TcCPSII* mRNA expression levels in WT, SKO, and DKO epimastigotes. The data shown are expressed as fold change and represent the mean ± SD of three independent experiments.

To examine the infectivity of host cells by metacyclic trypomastigotes, the remaining epimastigotes were killed by adding untreated (not heat-inactivated) FBS, as previously described [13]. The trypomastigotes were collected by centrifugation at 800g for 5 min in 15-ml polypropylene tubes to remove cell debris. The resulting supernatant was centrifuged at 1500g for 10 min at 4 °C, and the pellet containing trypomastigotes was washed three times with 10 ml of DMEM by repeated suspension and centrifugation. The purified trypomastigotes were counted on an improved Neubauer hemocytometer and used for experiments.

2.3. Generation of the knockout DNA cassettes for TcCPSII

We constructed two gene-knockout cassettes comprising the 5′ flanking region of TcCPSII, the neomycin phosphotransferase II gene (neo^R) or hygromycin B phosphotransferase gene (hyg^R), and an internal sequence from the TcCPSII gene (nucleotides +1000 to +2000) to allow disruption of the TcCPSII loci by homologous recombination (Fig. 1A). The knockout cassettes were constructed using a MultiSite Gateway® Three-Fragment Vector Construction Kit (Invitrogen) [14]. The pDEST/TcCPSII_Neo^R plasmid was constructed by amplifying the 5′ flanking sequence of TcCPSII (0.41 kb) using a primer set (sense, 5′-GGGGACAACTTTGTATA-GAAAAGTTGGAATTCGCGTCTTCCTTTTTTTCTTCCTTTTCTTTT-3′ and antisense, 5′-GGGGACTGCTTTTTTGTACAAACTTGTGTTTTACTTTTT-TATGTTTTGTGTTACTG-3′; the EcoRI site is underlined), KOD-Plus-Neo (TOYOBO), and T. cruzi Tulahuen genomic DNA as the template and was subsequently cloned into the entry vector (pDONR P4-P1R) via a BP reaction. Similarly, the coding region of TcCPSII (+1000 to +2000 bp) was amplified using a primer set (sense, 5′-GGGGACAGCTTTCTTGTACAAAGTGGTTCTCTGTACAGTTTCATCCG-3′ and antisense, 5′-GGGGACAACTTTGTATAATAAAGTTGGAATTCAGA-CGTGCATTAACCTCAATT-3′) and cloned into pDONR P2R-P3. The neo^R gene was amplified using a primer set (sense, 5′-GGGGAC-AAGTTTGTACAAAAAAGCAGGCTATGATTGAACAAGATGGATT-3′ and antisense, 5′-GGGGACCACTTTGTACAAGAAAGCTGGGTTCAGAAGA-ACTGGTCAAGAA-3′) and pTREX DNA as the template and cloned into entry vector pDONR 221. In order to generate the final plasmid, the three recombinant plasmids were subsequently transferred to a destination vector, pDEST R4-R3, according to the manufacturer's instructions. Finally, the knockout DNA cassette was excised from the plasmid backbone with EcoRI and used for electroporation.

To construct the pDEST/TcCPSII_Hyg^R plasmid, a 0.41-kb 5′ flanking sequence from TcCPSII was amplified using T. cruzi Tulahuen genomic DNA, a primer set (sense, 5′-GGGGACAAC-T TTGTATAGAAAAGTTGCAGCTGGCGTCTTCCTTTTTTTCTTCCTTTTC-TTTT-3′; the PvuII site for digestion is underlined and antisense, 5′-GGGGACTGCTTTTTTGTACAAACTTGTGTTTTACTTTTTTATGTTTTGT GTTACTG-3′) and KOD-Plus-Neo (TOYOBO) and cloned into the entry vector (pDONR P4-P1R) via a BP reaction. Similarly, a region of the TcCPSII ORF sequence (+1000 to +2000) was amplified from T. cruzi Tulahuen genomic DNA using a primer pair (sense, 5′-GGGGACAGCTTTCTTGTACAAAGTGGTTCTCTGTACAGTTTCATCCG-3′ and antisense, 5′-GGGGACAACTTTGTATAATAAAGTTGCAGCTGAG-ACGTGCATTAACCTCAATT-3′; the PvuII site for digestion is underlined) and cloned into pDONR P2R-P3. Using the pTEX-derived plasmid, p72hyg72 [15,16], as a template, the hyg^R gene was amplified with a primer set (sense, 5′-GGGGACAAGTTTGTACA-AAAAAGCAGGCTATGAAAAAGCCTGAACTCACC-3′ and antisense, 5′-GGGGACCACTTTGTACAAGAAAGCTGGGTTTCCTTTGCCCTCGGAC-GAGT-3′) and cloned into entry vector pDONR 221. The three entry clones were subsequently mixed with a destination vector (pDEST R4-R3) to generate the final plasmid by an LR reaction. The knockout DNA cassette was released from the plasmid backbone by PvuII digestion.

2.4. Transformation of T. cruzi using knockout DNA cassettes

About 1×10^7 early log-phase epimastigotes were suspended in 100 μl of Amaxa Basic® Parasite Nucleofector Kit 2 solution (Lonza). Transformation of the parasites was carried out using 10 μg of the knockout DNA cassette and the "U-033" program of an Amaxa Nucleofector Device (Lonza). Stable transformants were selected by incubating cells for 30–45 days in LIT medium containing 0.25 mg/ml G418 (for single-gene knockout [SKO] with neo^R) or 0.25 mg/ml G418 plus 0.25 mg/ml hygromycin B with 0.2 mM uracil (for double-gene knockout [DKO] with neo^R and hyg^R) and cloned by limiting dilution. Integration of the knockout cassette into the precise locus of the TcCPSII gene was confirmed by PCR using DNA cassette-specific sense primers (5′-ATCGCCTTCTTGAC-GAGTTCT-3′ for neo^R and 5′-ACTCGTCCGAGGGCAAAGGAA-3′ for hyg^R) and the TcCPSII-specific antisense primer (5′-CATTGTTGT-CTTGGTGACCCC-3′;+2101 to +2122 bp).

2.5. Real-time PCR

Total RNA was isolated from wildtype (WT), CPSII SKO, and CPSII DKO epimastigotes using Agilent Total RNA Isolation mini kits (Agilent Technologies, Santa Clara, CA). Subsequently, cDNA was prepared by reverse transcription using the SuperScript III First-Strand Synthesis System for RT-PCR (Invitrogen). Real-time PCR was performed using an Applied Biosystems 7500 Real-Time PCR System (Applied Bio Systems, Foster City, CA) and the following primers (TcCPSII-specific sense, 5′-TGGCCTTTTTATTTCCAACG-3′ and antisense, 5′-CGATGGCCGTACTTCATCTT-3′; T. cruzi beta tubulin-specific sense, 5′-TTTGTCGGCAACAACACCTG-3′ and antisense, 5′-CTAGTACTGCTCCTCCTCGT-3′).

3. Results and discussion

3.1. Construction of TcCPSII-knockout T. cruzi

T. cruzi is a diploid organism [17]. We previously demonstrated that the TcCPSII gene is a single-copy gene in T. cruzi Tulahuen and occurs at two gene loci per cell [6]. Thus, we aimed to generate TcCPSII-knockout parasites in order to investigate the physiological relevance of the de novo pyrimidine biosynthesis pathway in T. cruzi.

We constructed two gene knockout cassettes comprising the 5′ flanking region of TcCPSII, the neomycin phosphotransferase II gene (neo^R) or hygromycin B phosphotransferase gene (hyg^R), and the coding region of the TcCPSII gene (+1000 to +2000 bp) to allow disruption of the TcCPSII loci by homologous recombination (Fig. 1A). Integration of the knockout cassettes was confirmed by PCR using a sense primer specific for the resistance marker gene and an antisense primer specific for a region outside the 3′ cassette (Fig. 1B and C). For cloning of the DKO parasites, the culture medium was supplemented with uracil in order to complement the defect due to loss of the CPSII gene.

We analyzed the expression levels of TcCPSII transcripts in WT, SKO, and DKO parasites by real-time RT-PCR (Fig. 1D). A reduction in expression levels of approximately 50% was observed for the SKO parasites, which was directly proportional to the copy number of the functional TcCPSII gene. Moreover, transcription of TcCPSII in DKO parasites was at trace levels, indicating that DKO parasites are TcCPSII-null mutants.

3.2. Physiological importance of TcCPSII for the growth of T. cruzi epimastigotes

We investigated the physiological importance of de novo pyrimidine biosynthesis in epimastigotes by comparing the growth of

WT, SKO, and DKO epimastigotes in LIT medium supplemented with 10% FBS. The parasite growth curves for 9 days of cultivation are shown in Fig. 2. While the growth rates were almost identical for the first 6 days of cultivation, significant suppression of the growth of both SKO and DKO parasites was observed after 9 days of cultivation. Notably, the growth of the DKO parasites was more severely impaired than the growth of SKO parasites.

The addition of uracil (final concentration of 500 μM) rescued the growth defect of DKO epimastigotes to a level comparable to that of SKO parasites between days 7 and 9 (Fig. 2). Therefore, since the LIT medium appeared to contain a sufficient amount of pyrimidine precursors to support the growth of CPSII-knockout parasites during the early stages of cultivation, these results suggests that epimastigotes preferentially consume pyrimidine precursors in the medium during the first 6 days of cultivation and subsequently depend on de novo pyrimidine biosynthesis due to the absence of precursors after 7 days of cultivation.

To further confirm that the growth defect of DKO parasites was due to the lack of CPSII activity, we attempted to rescue parasites by overexpression of TcCPSII. The DKO and WT epimastigotes were transformed using a trypanosomal expression plasmid, pTREX [18], which carries the TcCPSII gene. However, we were unable to obtain transgenic parasites neither for the DKO nor for the WT background, suggesting that overexpression of TcCPSII is highly toxic for the parasites. Furthermore, we found that a high concentration of uracil (>500 μM) impaired the growth of parasites (data not shown). Therefore, as previously reported [3], both de novo pyrimidine biosynthesis and salvage pathways were shown to be physiologically active in epimastigotes. Moreover, we found that CPSII is required for parasite growth under culture conditions of insufficient salvage substrates.

During the life cycle of T. cruzi, epimastigotes transform into metacyclic trypomastigotes, which represent a transmission stage from the insect vector to mammalians. Metacyclogenesis is also inducible in conditioned medium lacking pyrimidine precursors [9]. Thus, we examined whether a pyrimidine supply is required for transformation of CPSII-SKO and DKO parasites. We compared the efficacy of metacyclogenesis of SKO, DKO, and WT parasites and found no significant difference between the groups (data not shown). Therefore, these results suggest that nucleotide synthesis is not critical for the process of metacyclogenesis.
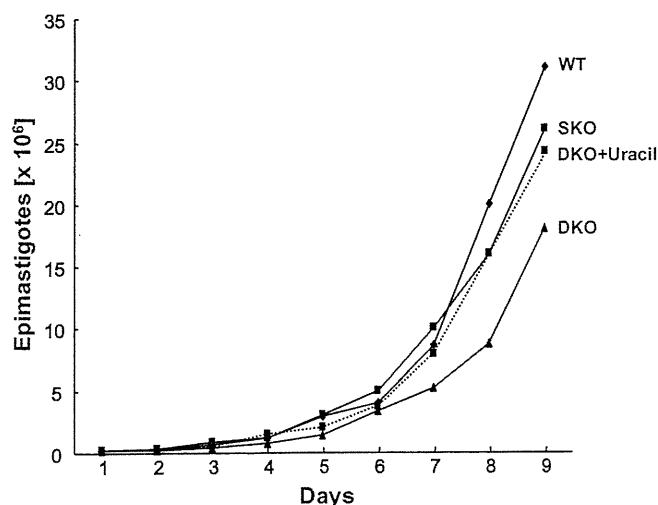
3.3. Physiological importance of TcCPSII for T. cruzi amastigote growth in the host cell

In general, pyrimidine de novo biosynthesis is particularly important in rapidly growing cells [7]. Since T. cruzi amastigotes are only proliferative in mammalian hosts, we examined whether CPSII and the de novo pyrimidine biosynthesis pathway are required for the growth of amastigotes.

We infected 3T3-Swiss fibroblast cells with metacyclic trypomastigotes from WT, SKO, or DKO parasites at an MOI of 0.26, and the average number of intracellular amastigotes per infected cell was compared between the groups. Multiple infections of a single host cell by metacyclic trypomastigotes were negligible under the experimental conditions employed (data not shown). The amastigote counts were significantly reduced for SKO and DKO parasites in a dose-dependent manner (Fig. 3), suggesting that de novo pyrimidine biosynthesis is more important for amastigotes than epimastigotes.

Extracellular amastigotes incorporate pyrimidine bases and nucleosides to a significantly lesser extent compared with epimastigotes and trypomastigotes [3]. In addition, the average concentrations of uridine in mammalian tissues and plasma are estimated to be of the micromolar order [4,19]. Therefore, amastigotes are likely to rely on de novo pyrimidine biosynthesis. We observed that DKO amastigotes appeared to replicate approximately two times after 4 days of cultivation. These results indicate that the concentrations of intracellular pyrimidine precursors are insufficient to support amastigote replication, resulting in the dependence on de novo pyrimidine biosynthesis. Moreover, our observations are in good agreement with a study on another intracellular parasite, Toxoplasma gondii, which also has limited pyrimidine salvage ability [20]. Indeed, the CPSII-null mutant of this apicomplexan parasite was only able to replicate inside the host cell in culture medium supplemented with >200 μM uracil as a pyrimidine source.

We have previously shown that disruption of 2 of the 3 loci for the dihydroorotate dehydrogenase (DHOD) gene, encoding the fourth enzyme of the de novo pyrimidine biosynthesis pathway, led to the gradual death of T. cruzi epimastigotes, which were no longer viable 2 weeks later [16]. Furthermore, the addition of uridine, cytidine, and thymidine (200 μM each) to the medium did not enable growth of DHOD DKO epimastigotes. While these
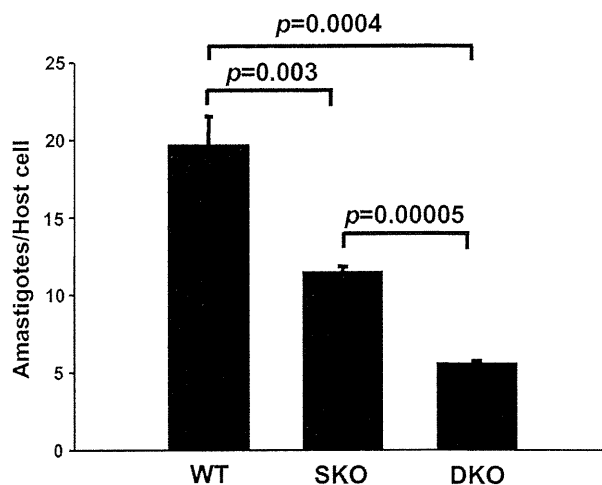
Fig. 2. Physiological role of CPSII in the growth of T. cruzi epimastigotes. A total of 1×10^6 WT, SKO, or DKO epimastigotes were grown in liver infusion tryptose (LIT) medium, and the average number of parasites from three independent experiments is shown. DKO + uracil represents DKO parasites grown in the presence of 500 μM uracil.

Fig. 3. Physiological role of CPSII in the growth of T. cruzi amastigotes. A total of 1.5×10^5 3T3-Swiss Albino cells were infected with 4×10^4 WT, SKO, or DKO metacyclic trypomastigotes (MOI, 0.26) and cultured for 4 days. The average number of parasites per infected cell is shown, and data represent the mean ± SD of three independent experiments.

findings differ from the phenotype of CPSII DKO epimastigotes, the phenotypic difference between CPSII and DHOD KO parasites may be attributed to the coupled reaction of DHOD. In *T. cruzi*, catalysis of the oxidation of dihydroorotate by DHOD is coupled with the reduction of fumarate to succinate. In addition, this reaction is reversible. Therefore, it is likely that the fumarate-reductase activity of DHOD—as well as succinate production by its reverse reaction—contributes to maintenance of the redox balance in epimastigotes. Moreover, *T. cruzi* DHOD may use not only dihydro-orotate but also other unidentified substrates as electron donors/acceptors for succinate/fumarate metabolism.

Thus, we conclude that the *de novo* pyrimidine biosynthesis pathway is critical for intracellular replication of *T. cruzi*. Our findings provide insight into CPSII and the pyrimidine metabolic pathway, which represents a promising target for chemotherapy. The screening of chemical compound libraries by using recombinant enzymes and bioassay systems may facilitate the identification of seed compounds for drug development against Chagas disease.

Acknowledgments

References

[1] A. Rassi Jr., A. Rassi, J.A. Marin-Neto, Chagas disease, Lancet 375 (2010) 1388–1402.

[2] Z. Brener, Biology of *Trypanosoma cruzi*, Annu. Rev. Microbiol. 27 (1973) 347–382.

[3] W.E. Gutteridge, M. Gaborak, A re-examination of purine and pyrimidine synthesis in the three main forms of *Trypanosoma cruzi*, Int. J. Biochem. 10 (1979) 415–422.

[4] T.W. Traut, Physiological concentrations of purines and pyrimidines, Mol. Cell Biochem. 140 (1994) 1–22.

[5] D.J. Hammond, W.E. Gutteridge, UMP synthesis in the kinetoplastida, Biochim Biophys Acta 718 (1982) 1–10.

[6] G. Gao, T. Nara, J. Nakajima-Shimada, T. Aoki, Novel organization and sequences of five genes encoding all six enzymes for de novo pyrimidine biosynthesis in *Trypanosoma cruzi*, J. Mol. Biol. 285 (1999) 149–161.

[7] T. Aoki, G. Weber, Carbamoyl phosphate synthetase (glutamine-hydrolyzing): increased activity in cancer cells, Science 212 (1981) 463–465.

[8] J. Nakajima-Shimada, Y. Hirota, T. Aoki, Inhibition of *Trypanosoma cruzi* growth in mammalian cells by purine and pyrimidine analogs, Antimicrob. Agents Chemother. 40 (1996) 2455–2458.

[9] E. Gluenz, M.C. Taylor, J.M. Kelly, The *Trypanosoma cruzi* metacyclic-specific protein Met-III associates with the nucleolus and contains independent amino and carboxyl terminal targeting elements, Int. J. Parasitol. 37 (2007) 617–625.

[10] J. Cardoso, M.J. Soares, R.F. Menna-Barreto, R. Le Bloas, V. Sotomaior, S. Goldenberg, M.A. Krieger, Inhibition of proteasome activity blocks *Trypanosoma cruzi* growth and metacyclogenesis, Parasitol. Res. 103 (2008) 941–951.

[11] J.J. Sullivan, Metacyclogenesis of *Trypanosoma cruzi* in vitro: a simplified procedure, Trans. R Soc. Trop. Med. Hyg. 76 (1982) 300–303.

[12] J. Cardoso, M.J. Soares, In vitro effects of citral on *Trypanosoma cruzi* metacyclogenesis, Mem. Inst. Oswaldo Cruz 105 (2010) 1026–1032.

[13] N. Nogueira, C. Bianco, Z. Cohn, Studies on the selective lysis and purification of *Trypanosoma cruzi*, J. Exp. Med. 142 (1975) 224–229.

[14] D. Xu, C.P. Brandán, M.A. Basombrio, R.L. Tarleton, Evaluation of high efficiency gene knockout strategies for *Trypanosoma cruzi*, BMC Microbiol. 9 (2009) 90.

[15] T. Nozaki, G.A.M. Cross, Functional complementation of glycoprotein 72 in a *Trypanosoma cruzi* glycoprotein 72 null mutant, Mol. Biochem. Parasitol. 67 (1994) 91–102.

[16] T. Annoura, T. Nara, T. Makiuchi, T. Hashimoto, T. Aoki, The origin of dihydroorotate dehydrogenase genes of kinetoplastids, with special reference to their biological significance and adaptation to anaerobic, parasitic conditions, J. Mol. Evol. 60 (2005) 113–127.

[17] N.M. El-Sayed, P.J. Myler, D.C. Bartholomeu, D. Nilsson, G. Aggarwal, A.N. Tran, et al., The genome sequence of *Trypanosoma cruzi*, etiologic agent of Chagas disease, Science 309 (2005) 409–415.

[18] M.P. Vazquez, M.J. Levin, Functional analysis of the intergenic regions of TcP2beta gene loci allowed the construction of an improved *Trypanosoma cruzi* expression vector, Gene 239 (1999) 217–225.

[19] G.J. Peters, G. Codacci-Pisanelli, Physiological and pharmacological sources of plasma uridine, Paths to Pyrimidines 3 (1995) 31–41.

[20] B.A. Fox, D.J. Bzik, De novo pyrimidine biosynthesis is required for virulence of *Toxoplasma gondii*, Nature 415 (2002) 926–929.
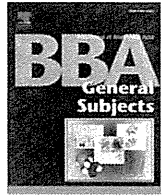
Review

Mitochondrial fumarate reductase as a target of chemotherapy: From parasites to cancer cells ☆

Chika Sakai [a], Eriko Tomitsuka [a,b], Hiroyasu Esumi [b], Shigeharu Harada [c], Kiyoshi Kita [a,*]

[a] Department of Biomedical Chemistry, Graduate School of Medicine, The University of Tokyo, Tokyo 113-0033, Japan
[b] Cancer Physiology Project, Investigative Treatment Division, National Cancer Center Research Institute East, 6-5-1 Kashiwanoha, Kasiwa, Chiba 277-8577, Japan
[c] Department of Applied Biology, Graduate School of Science and Technology, Kyoto Institute of Technology, Kyoto 606-8585, Japan

ABSTRACT

Recent research on respiratory chain of the parasitic helminth, Ascaris suum has shown that the mitochondrial NADH-fumarate reductase system (fumarate respiration), which is composed of complex I (NADH–rhodoquinone reductase), rhodoquinone and complex II (rhodoquinol–fumarate reductase) plays an important role in the anaerobic energy metabolism of adult parasites inhabiting hosts. The enzymes in these parasite-specific pathways are potential target for chemotherapy. We isolated a novel compound, nafuredin, from Aspergillus niger, which inhibits NADH-fumarate reductase in helminth mitochondria at nM order. It competes for the quinone-binding site in complex I and shows high selective toxicity to the helminth enzyme. Moreover, nafuredin exerts anthelmintic activity against Haemonchus contortus in in vivo trials with sheep indicating that mitochondrial complex I is a promising target for chemotherapy. In addition to complex I, complex II is a good target because its catalytic direction is reverse of succinate–ubiquionone reductase in the host complex II. Furthermore, we found atpenin and flutolanil strongly and specifically inhibit mitochondrial complex II.
Interestingly, fumarate respiration was found not only in the parasites but also in some types of human cancer cells. Analysis of the mitochondria from the cancer cells identified an anthelminthic as a specific inhibitor of the fumarate respiration. Role of isoforms of human complex II in the hypoxic condition of cancer cells and fetal tissues is a challenge. This article is part of a Special Issue entitled Biochemistry of Mitochondria, Life and Intervention 2010.

© 2011 Elsevier B.V. All rights reserved.

1. Introduction

In the general understanding of bioenergetics of higher eukaryotes, oxygen is a most important terminal electron acceptor of mitochondrial respiratory chain (Fig. 1). The major function of the aerobic respiratory chain is the electrogenic translocation of protons out of the mitochondrial or bacterial membrane to generate the proton motive force that drives ATP synthesis by F_oF_1-ATPase. This mechanism of oxidative phosphorylation is conserved basically from aerobic bacteria to human mitochondria. However, recent study on the respiratory chain of the lower eukaryotes which reside

micro-aerophilic environment has shown that the mitochondrial NADH-fumarate reductase system (fumarate respiration) plays an important role in the anaerobic energy metabolism [1]. This system is composed of complex I (NADH-quinone reductase), low potential quinone species and complex II (quinol–fumarate reductase: QFR).

Fumarate respiration is well known electron transport chain in the anaerobic bacteria [2]. Reducing equivalent of NADH is transferred to low potential quinone such as naphthoquione by complex I and finally is oxidized by fumarate by the fumarate reductase activity of complex II which is a reverse reaction of succinate–ubiquinone reductase (SQR) activity of complex II. By using this respiratory chain, bacteria are able to synthesize ATP even in the absence of oxygen. Recently our study of parasitic nematode, Ascaris suum, showed fumarate respiration also plays an important role in the anaerobic energy metabolism of adult worms, which reside in the host small intestine where oxygen tension is low [1]. Although fumarate reductase activities of bacterial and mitochondrial complex IIs are the same reaction, evolutional positions of each enzyme are quite different. All four subunits of complex II in adult A. suum are more closely related to the bacterial and mitochondrial SQR than to bacterial QFR [3–5].
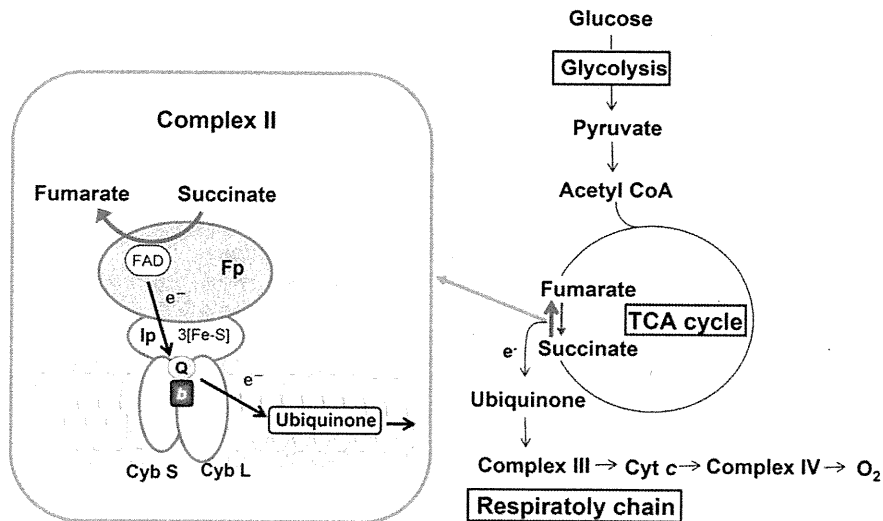
Fig. 1. Complex II is the member of TCA cycle and respiratory chain.Complex II catalyzes the oxidation of succinate to fumarate in the TCA cycle and transports the electron generated by this oxidation to ubiquinone in the respiratory chain. Generally, complex II consists of four subunits. Flavoprotein (Fp) subunit contains a flavin adenine dinucleotide prosthetic group and iron–sulfur protein (Ip) subunit contains three iron–sulfur clusters. There are two hydrophobic cytochrome*b* (Cyb L, Cyb S) subunits. The succinate binding site is located in Fp subunit, while the quinone binding site is formed by three subunits, Ip, Cyb L and CybS. Complex II also catalyzes the reduction of fumarate, a reverse-reaction of succinate dehydrogenase, in the respiratory chain of mitochondria from anaerobic animals, such as *Ascaris suum*, as well as anaerobic bacteria.

Thus, mitochondrial QFR is a new enzyme evolved by "reverse evolution" of SQR rather than direct evolution from bacterial QFR [6].

Recently our study has revealed that fumarate respiration functions in some human cancer cells and supports a survival of cancer cells in low nutrition and low oxygen conditions [7,8]. Furthermore, we found complex II with high QFR activity produces reactive oxygen species (ROS) [9]. ROS has been reported to contribute to proliferation and metastasis of cancer cells via the stabilization of hypoxia-inducible factor-1 (HIF-1) [10]. In addition, succinate produced by fumarate respiration also stabilize HIF-1 by the product inhibition of HIF prolyl hydroxylase, which catalyzes the oxygen-dependent hydroxylation of the conserved proline residues in HIF-1 α [11]. Thus, the relationship between accumulation of succinate resulted from functional defect of human complex II by the mutation of the subunits and carcinogenesis has recently become a focus of research [8].

As fumarate respiration is essential for the growth and survival of the parasites and some cancer cells, it should be a promising target of chemotherapy for both parasitic diseases and cancer. In this review, we focus on recent advances in the study of parasite and human mitochondrial fumarate respiration and complex II which is an important component of the system [8].

2. Fumarate respiration of parasite mitochondria

2.1. Life cycle of A. suum and changes in respiratory chain

A. suum is the most widely known parasite, and has been studied as a representative of human and livestock parasites [12–14]. Because of its large size, A. suum is ideal for the study including biochemical analysis. Adult A. suum resides in the small intestine of mammals, and the female produces between 200,000 and 400,000 fertilized eggs per day (Fig. 2). Eggs are excreted with feces and become mature eggs containing infectious 3rd stage larvae (L3) in about 2–3 weeks at normal temperature. The eggs reach the small intestine and hatch, when orally ingested by a host. A hatched larva invades the intestinal wall, and migrates to the liver, lung, trachea, and pharyngeal region, and finally returns to the intestine via the esophagus and stomach, and becomes an adult worm. In humans, the larvae of A. suum migrate to several organs including liver and lung and cause a wide variety of nonspecific symptoms such as general malaise, cough, liver

dysfunction, hypereosinophilia with hepatomegaly and/or pneumonia. The oxygen concentration of the small intestine (~5%) is approximately 25% of that outside the body, and provides an environment of low oxygen tension in which the energy metabolism of the adult differs considerably from that of the larvae and the host (Fig. 3). The phosphoenolpyruvate carboxykinase (PEPCK)–succinate pathway, an anaerobic glycolytic pathway, operates in the adult worm, producing ATP under such a hypoxic conditions. This system is used by many other parasites such as Echinococcus multilocularis [15], and has also been observed in the adductor muscle of oysters and other bivalves that require energy conversion under anaerobic conditions. It is therefore considered to be a very common pathway for energy metabolism in adaptation to hypoxic environment [16,17].

The first half of the PEPCK–succinate pathway is the same glycolytic pathway found in mammals, in which phosphoenolpyruvate (PEP) is produced. In contrast to aerobic metabolism in mammals involving the conversion of PEP to pyruvate by pyruvate kinase, the A. suum adult fixes CO_2 with PEPCK to produce oxaloacetate (OAA). The OAA is converted to malate by the reverse reaction of malate dehydrogenase and transported into the mitochondria to produce pyruvate and fumarate. The NADH formed during production of pyruvate from malate is used in the reduction of fumarate to succinate. The NADH-fumarate reductase system, which is the anaerobic electron transport system characteristic of adult A. suum mitochondria, is the final step of this pathway. Unique property of this pathway is discussed in the next section.

In contrast to larvae which require oxygen for their development and possess the respiratory system to be almost the same as that of mammals, cytochrome c oxidase (complex IV) is not found in the respiratory chain of adult A. suum mitochondria, and the content of ubiquinol–cytochrome c reductase complex (complex III) is extremely low [18]. In addition to the enzymes, quinone species in the mitochondria also change during the life cycle of A. suum. In contrast to adult mitochondria, in which the low-potential rhodoquinone (RQ; $Em' = -63mV$) is the major quinone, ubiquinone (UQ; $Em' = +110mV$) is the major quinone of larvae (Fig. 4A) [19]. A combination of SQR and UQ, and that of QFR and a low-potential quinone, such as RQ or menaquinone (MK), is also observed in Escherichia coli and other bacteria during metabolic adaptation to changes in
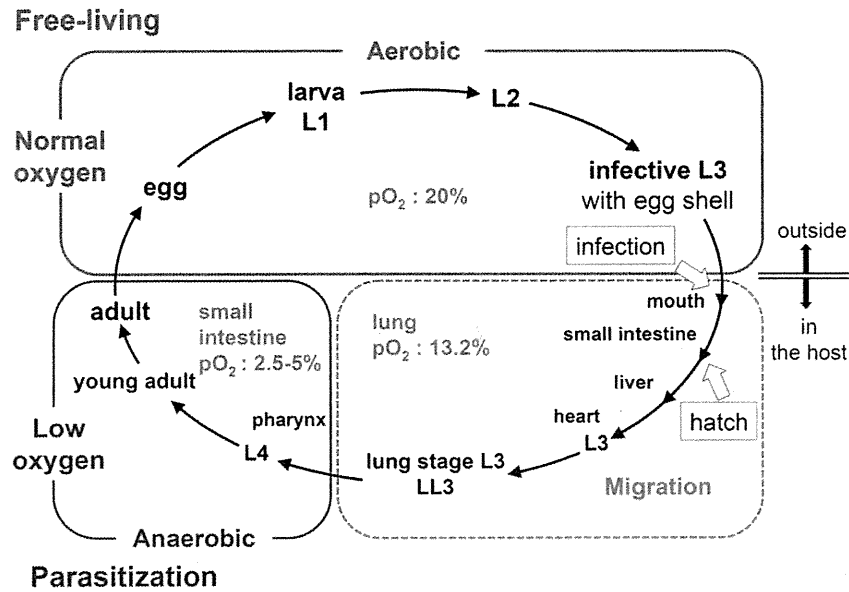
Free-living

Fig. 2. Life cycle of *Ascaris suum*.Fertilized eggs grow to be infective L3 under aerobic environment. Infective L3 larvae are ingested by the host, reach the small intestine and hatch there. Afterwards, larvae migrate into host body (liver, heart, lung, pharynx), and finally migrate back to the small intestine and become adults. In the host small intestine, the oxygen concentration is low ($pO_2 = 2.5$–5%) compared with the exogenous environment ($pO_2 = 20\%$). The metabolic pathway of *A. suum* changes dramatically during its life cycle, to adapt to changes in the environmental oxygen concentration [6].

oxygen supply [20,21]. Lower potential of RQ and MK is favorable for the electron transfer from NADH to fumarate (Fig. 4B). In this way, UQ participates in aerobic metabolism in *A. suum* larva, whereas RQ participates in anaerobic metabolism in adult *A. suum*.

Although studies have shown a clear difference in energy metabolism between larval and adult *A. suum* mitochondria, little is known about changes in the properties of mitochondria during migration of *A. suum* larvae in the host. As described later, examination of the changes in enzymatic characteristics and subunit composition of *A. suum* larval complex II from lung stage L3 (LL3) larvae obtained from rabbits showed that properties of LL3 mitochondria differed from those of L3 and adult mitochondria [22]. Protein chemical

analysis revealed that the change in complex II begins with the anchor subunit, and then occurs in the catalytic subunit. Thus, *A. suum* is able to adapt to changes in oxygen concentration in the environment during its life cycle by dynamic change of respiratory chain.

2.2. NADH-fumarate reductase system (fumarare respiration) of A. suum adult

The final step of the PEPCK–succinate pathway, which plays such an important role in the anaerobic energy metabolism of the *A. suum* adult, is catalyzed by the NADH-fumarate reductase system as
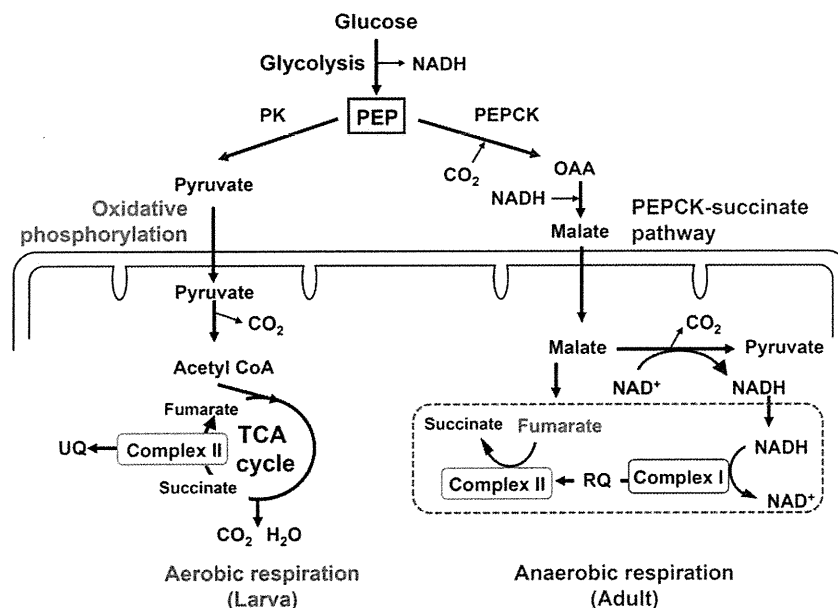

Fig. 3. Glucose metabolism of *A. suum* larval and adult mitochondria.The metabolic pathway of *A. suum* adult has a unique anaerobic electron transport system, NADH-fumarate reductase system. In the phospho*enol*pyruvate carboxykinase (PEPCK)–succinate pathway, phospho*enol*pyruvate (PEP) produced by a glycolytic process is carboxylated to form oxaloacetate and is then reduced to malate. The cytosolic malate is transported into the mitochondria, where it is first reduced to fumarate, and finally to succinate by the rhodoquinol–fumarate reductase activity of complex II. The terminal step is catalyzed by the NADH-fumarate reductase system (boxed in broken lines) comprised of complex I, rhodoquinone (RQ), and complex II. PEP, phosphoenolpyuvate; PEPCK, phoshoenolpyruvate carboxykinase; OAA, oxaloacete [6].

A Ubiquinone   Rohdoquinone

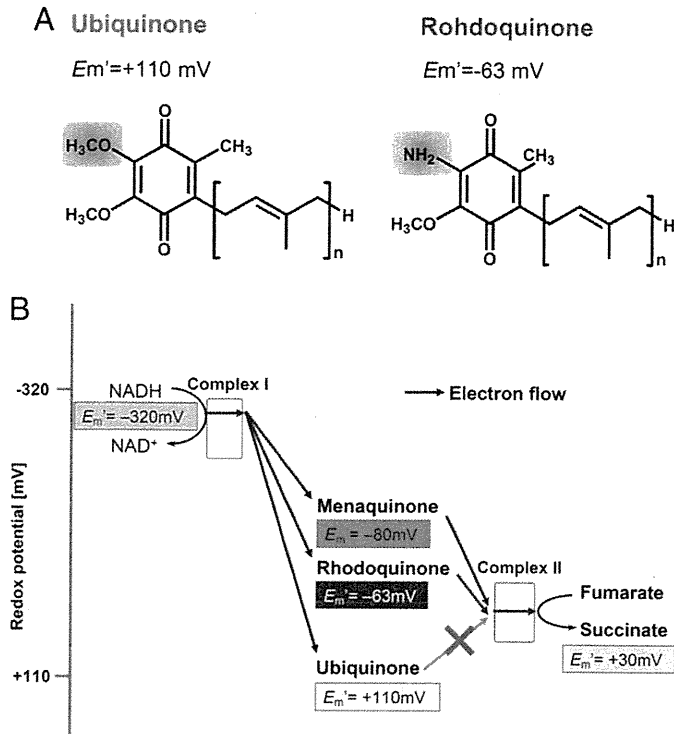$Em' = +110$ mV $Em' = -63$ mV

B

Fig. 4. Chemical structure and redox potentials of the quinones. A. Chemical structures of UQ and RQ. n, numbers of isoprenyl groups in side-chain. B. Redox potentials of quinones and substrates.

Fig. 5. NADH-fumarate reductase System of *A. suum* as a target of chemotherapy. The differences in energy metabolisms between host and helminths are an attractive therapeutic targets for helminthiasis. NADH-fumarate reductase is a part of a unique respiratory system in parasitic helminths and is the terminal step of the phosphoenolpyruvate carboxykinase–succinate pathway, which is found in many anaerobic organisms. NADH-fumarate reductase system is a potential target for chemotherapy. Nafuredin was found to be competitive inhibitor for rhodoquinone binding site of *A. suum* complex II [1].

described in the previous section. This system is also called "fumarate respiration". The low-potential rhodoquinone transfers reducing equivalent of NADH via complex I to complex II, and finally succinate is produced by quinol fumarate reductase (QFR) activity of complex II. The merit of this system is to synthesize ATP using the coupling site of complex I even in the absence of oxygen, although its energy efficiency is low (Fig. 5).

A similar anaerobic respiration system exists in the mitochondria of many other parasites, and has also been found in bacteria. Extensive studies of bacteria, including *E. coli*, have revealed the details of this system [23,24]. In *E. coli*, there are two types of complex II, and QFR encoded by the *frd* operon is induced under anaerobic conditions. A low molecular weight mediator between complex I and complex II is menaquinone (MK; $Em' = -80$ mV), a low-potential naphthoquinone, in the *E. coli* fumarate respiration. In contrast, under aerobic conditions, SQR encoded by *sdh* operon that catalyzes oxidation of succinate is induced [25]. SQR is a dehydrogenase complex in the respiratory system as well as an enzyme in the TCA cycle, and directly connects these systems in aerobic energy metabolism.

Thus, two different enzymes (complex II) are present in *E. coli*, and the bacteria maintain homeostasis of the energy metabolism by controlling the synthesis of these enzymes in response to the environmental oxygen supply. How about the complex IIs of *A. suum*? Biochemical and molecular biological analyses showed *A. suum* also possesses two different complex IIs. However, subunit compositions and expression patterns are more complicated in the parasite complex II.

3. Complex IIs of *A. suum* mitochondria

3.1. Multiple complexes II in A. suum mitochondria

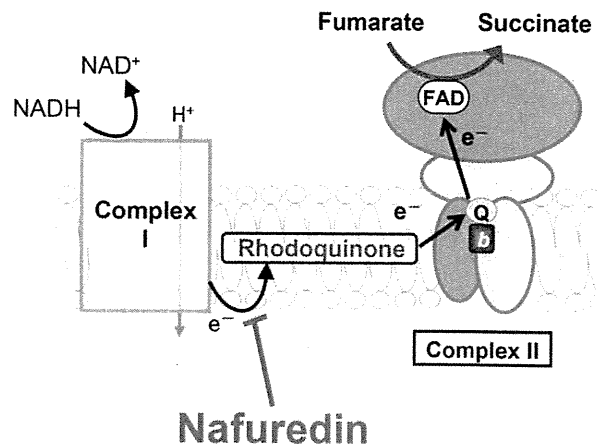The complex II superfamily comprises succinate–quinone reductase (SQR) and quinol–fumarate reductase (QFR), which catalyze the interconversion of succinate and fumarate with quinone and quinol. SQR is a component of the aerobic respiratory chain as well as the tricarboxylic acid (TCA) cycle [26]. QFR is a component of the anaerobic respiratory chain in anaerobic and facultative anaerobic bacteria [27] and lower eukaryotes [6,28]. SQR and QFR complexes generally consist of four subunits referred to as the flavoprotein subunit (Fp), iron–sulfur subunit (Ip), cytochrome *b* large subunit (CybL), and cytochrome *b* small subunit (CybS). The Fp and Ip subunits comprise the catalytic domain of the enzyme. The Fp subunit has a FAD as a prosthetic group and contains the dicarboxylate-binding site. The Ip subunit generally contains three iron–sulfur clusters $[2Fe-2S]^{2+,1+}$, $[4Fe-4S]^{2+,1+}$, and $[3Fe-4S]^{1+,0}$. Subunits CybL and CybS, with heme *b* as the prosthetic group, form the anchor domain of the enzyme. This anchors the catalytic domain to the inner mitochondrial membrane and also serves as the quinone oxidation/reduction site [29].

Our previous study showed that *A. suum* mitochondria express stage-specific isoforms of complex II (SQR in larvae/QFR in adult) (Fig. 6). The Fp and CybS in adult complex II differ from those of infective third stage larval (L3) complex II. In contrast, there is no difference in the iron-sulfur cluster (Ip) and CybL between adult and L3 isoforms of complex II. However, recent analysis of the changes that occur in the respiratory chain of *A. suum* larvae during their migration in the host, we found that enzymatic activity, quinone content and complex II subunit composition in mitochondria of lung stage L3 (LL3) *A. suum* larvae is different from those of L3 and adult [22]. Quantitative analysis of quinone content in LL3 mitochondria showed that ubiquinone is more abundant than rhodoquinone. Interestingly, the results of two-dimensional bule-native/sodium dodecyl sulfate polyacrylamide gel electrophoresis analyses showed that LL3 mitochondria contained larval Fp (Fp^L) and adult Fp (Fp^A) at a ratio of 1:0.56, and that most LL3 CybS subunits were of the adult form (CybS^A). This result clearly indicates that the rearrangement of complex II begins with a change in the isoform of the anchor CybS subunit, followed by a similar change in the Fp subunit. At any event, the NADH-fumarate reductase activity of *A. suum* adult worms (~100 nmol/min/mg) are much higher than that of the mammalian host (2~5 nmol/min/mg).

3.2. ROS production from complex II

Mitochondrial respiratory chain is a significant source of cellular ROS. Impairment of the respiratory chain complexes is known to
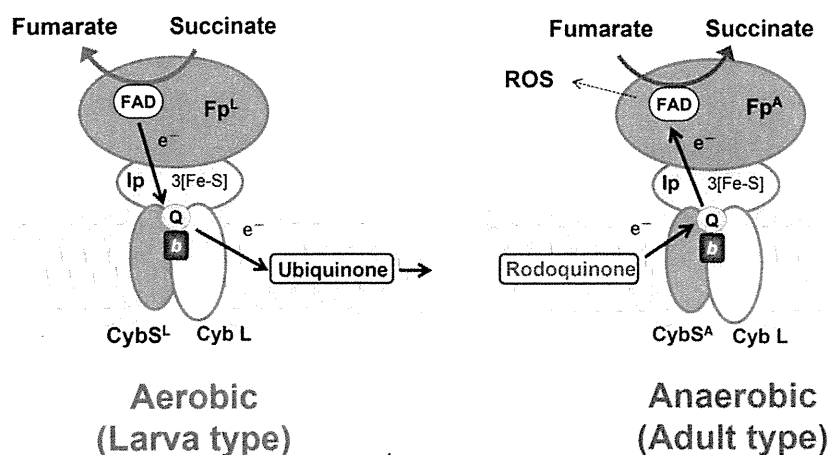
Fig. 6. Schematic representation of A. suum complexes II from larva type and adult type.The mitochondrial metabolic pathway of the parasitic nematode A. suum changes dramatically during its life cycle, to adapt to changes in the environmental oxygen concentration. A. suum mitochondria express stage-specific isoforms of complex II. While there is no difference in the isoforms of the Ip and cybL subunits of complex II between L3 larvae and adult A. suum, they have different isoforms of complex II subunits Fp (larval, Fp^L; adult, Fp^A) and cybS (larval, cybS^L; adult, cybS^A) in A. suum adult respiratory chain, complex II produces high amount ROS [29].

increase the cellular ROS production [30]. In general, complexes I and III are considered as the two major sites of superoxide and hydrogen peroxide production in the respiratory chain [30–33]. Interestingly, our results show that complex II is the main site of ROS production in A. suum adult respiratory chain [9].

Analysis of submitochondrial particles for superoxide (O_2^-) production using superoxide dismutase inhibitable acetylated cytochrome c reduction, and hydrogen peroxide production using catalase inhibitable amplex red oxidation, in the presence and absence of respiratory chain inhibitors, showed the contribution from both the FAD site and quinone-binding site of complex II to produce O_2^- and H_2O_2 when succinate is oxidized under aerobic conditions. Considering the conservation of amino acid residues critical for the enzyme reaction between A. suum complex II and mitochondrial SQR, our results show the ROS production from more than one site in mitochondrial complex II linked with subtle differences in the amino acid sequences of the enzyme complex.

A. suum adult complex II is a good model to study the mechanism of ROS production from mitochondrial complex II, since amino acid residues conserved among the catalytic domains in mitochondrial SQR enzymes are well conserved in this enzyme and it produces high levels of ROS. Absence of complex III and IV activities in its respiratory chain is an additional advantage of this model. These studies will provide further insight into the possibility of high levels of ROS production from both the FAD site and the Q site in the complex II of A. suum adult worm and help to understand the role of mutations in human complex II for carcinogenesis.

3.3. Specific inhibitors of complex II

The differences between parasite and host mitochondria described in this review hold great promise as targets for chemotherapy. For example, the anti-malarial drug Atovaquone, which was recently developed, acts on the mitochondrial respiratory chain [34]. Atovaquone is effective against chloroquine-resistant strains, [35]. The specific target is thought to be complex III, and biochemical analysis has shown that it acts on the ubiquinone oxidation site in the cytochrome b of complex III [36,37]. Such a chemotherapeutic approach is also applicable to the helminthes. It has been proposed that the fumarate respiration is the target of such drugs as bithionol and thiabendazole [38,39], but there is no clear biochemical or pharmaceutical evidence to support this idea. However, as described in the previous section, progress in the study of the NADH-fumarate reductase pathway permits screening of new anthelmintic compound.

Nafuredin, selectively inhibits helminth complex I at concentrations in the order of nanomoles [40] (Fig. 7). Kinetic analysis revealed that the inhibition by nafuredin is competitive against RQ (Fig. 5). These findings, coupled with the fact that helminth complex I uses both RQ and UQ as an electron acceptor, suggest that the structural features of the quinone reduction site of helminth complex I may differ from that of mammalian complex I. In fact, the inhibitory mechanism of quinazolines, which effectively kill the E. multilocularis protoscoleces, was competitive and partially competitive against RQ and UQ, respectively [41].

The most potent inhibitor of complex II, Atpenin A5, was found during the screening of inhibitors for A. suum complex II [42]. To our regret, IC$_{50}$ of Atpenin A5 for bovine complex II (3.6 nM) was lower than that for A. suum complex II (12 nM for QFR and 32 nM for SQR). However, further screening of inhibitors showed that flutolanil, a commercially available fungicide, specifically inhibits A. suum SQR [43] (Fig. 7). The IC$_{50}$ of flutolanil against A. suum and bovine SQR was 0.081 and 16 μM, respectively, indicating that flutolanil is a promising lead compound for anthelminthics. To enable rational drug optimization, a crystal of the A. suum QFR complexed with
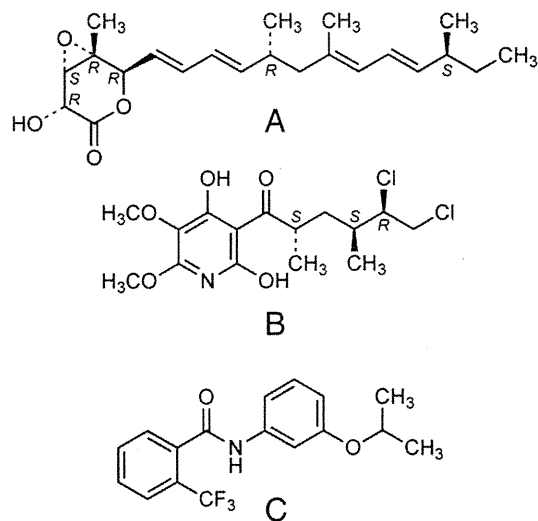

Fig. 7. Chemical structure of inhibitors of complex II.A. Nafuresin, a competitive inhibitor for the rhodoquinone binding site of A. suum complex II; B. Atpenin A5, a competitive inhibitor for the quinone binding site of complex II of many species; C. Fulutolanil, a competitive inhibitor for the quinone binding site of A. suum complex II.

flutolanil was prepared by soaking, and X-ray structure analysis has been performed. The current structural model of the flutolanil bound form of the A. suum QFR (Harada, unpublished observation) indicates that flutolanil is bound to the same site as those of the quinone binding observed in complex IIs from pig heart mitochondria (pdb code 1ZOY), E. coli (1NEK and 1L0V) and avian (1YQ4). The site of the pig enzyme, for example, is composed of ten residues highly conserved across amino acid sequences of these complex IIs; Pro169, Trp173 and Ile218 from the Ip subunit, Ile30, Trp35, Met39, Ser42, Ile43 and Arg46 from the CybL subunit, and Tyr91 from the CybS subunit. However, three residues, Trp35, Met39 and Ile53, are replaced by Pro65, Trp69 and Gly73, respectively, in A. suum QFR. The structures of the A. suum QFR together with those of QFRs from Wolinella succinogenes [24] and E. coli [23], and SQRs from E. coli [44], pig heart mitochondria [45], and avian heart mitochondria [46] should help clarify the structure–function relationship of complex II and provide useful information for the structure-based design of anthelminthics.

4. Fumarate respiration of human mitochondria

4.1. Human complex II

In human, many cases of diseases caused by mutations in subunits of complex II have been reported. Mutations found in the Ip, Cyb L or Cyb S are associated with the development of pheochromocytoma and paraganglioma [47–51]. It is suggested that the causes of tumorigenesis are ROS production from mutated complex II [52,53] or accumulation of succinate as a result of SQR inhibition [11]. Accumulated succinate inhibits HIF-1α prolyl hydroxylases in the cytosol, leading to stabilization and activation of HIF-1α. Thus, succinate can increase expression of genes that facilitate angiogenesis, metastasis, and glycolysis, ultimately leading to tumor progression. On the other hand, no patient with mutation in Fp linked to tumorigenesis has been reported. There are two Fp isoforms in human, which will be discussed later, and this is probably the reason why mutations in Fp are not directly linked to tumorigenesis. Instead, mutations in Fp are linked to severe metabolic disorders resulting from decreased activity of the TCA cycle and impairment of oxidative phosphorylation, although these are rare. These autosome-recessive disorders are manifested as childhood encephalopathy, myopathy, adult optic atrophy, and Leigh syndrome [54–57]. Recently, two new proteins, SDHAF1 (succinate dehydrogenase complex assembly factor 1) and SDHAF2, were found to be the first assembly factors of complex II [53,58]. It was suggested that mutations found in SDHAF1 may result in the reduction of assembled complex II and cause infantile leukoencephalopathy [58]. SDHAF2 is suggested to be required for the

incorporation of the flavin adenine dinucleotide cofactor (flavination) of SDHA (succinate dehydrogenase complex, subunit A, flavoprotein), and it is also necessary for complex II assembly and function [53]. Furthermore, the mutation found in SDHAF2 has been suggested to link to familial paraganglioma [53]

4.2. Isoforms of human complex II

In 2003, we found two isoforms of human Fp, type I and type II [59,60] (Fig. 8). These isoforms differ from each other only in two amino acid residues. Tyr 586 and Val 614 of type I Fp are replaced by Phe 586 and Ile 614 in type II Fp, respectively. Tyr 586 and Val 614 are well conserved among mammals' Fps and type II Fp is found only in human complex II (Fig. 9). Type I Fp gene has an exon–intron structure, while the structure of type II Fp gene has not been determined. The type II Fp gene is not found in the NCBI database and the location has not been clarified yet while type I Fp gene is located on chromosome 5p15 [59,60].

Complex II with type I Fp has isoelectric point (pI) of 6–7, whereas complex II with type II Fp shows its pI of 5–6. To explain the difference of pI values, several reports suggested the phosphorylation of amino acid residues in Fp subunit [7,61]. One of these residues, Tyr 500, is located close to Tyr 586, which is replaced by Phe in type II Fp (Fig. 10). Since the Tyr 586 Phe substitution will certainly destroy a hydrogen bond between Tyr 586 O_η and Glu 597 O_δ (3.13Å), the local structure around Tyr 586 as well as Tyr 500 phosphorylation status may be different between Fps of types I and II.

The result of biochemical analysis of complex II with each isoform, complex II with each Fp was found to have almost the same SQR specific activities. However, type II Fp has lower optimal pH than type I Fp and at optimal pH of type II Fp, K_m value for succinate of type II Fp is lower than type I Fp (Sakai unpublished data). It may be possible that different phosphorylation statuses of complex II with each isoform cause biochemical differences.

4.3. Expression of human complex II containing type II Fp

Our previous study on the expression of isoforms showed that both types were expressed in all the organs tested (liver, heart, skeletal muscle, brain and kidney) and expression of type I Fp was higher than that of type II Fp [59,60]. This tendency was also found in the cultured cells such as Fibroblast, Myoblast, Human Umbilical Vein Endothelial Cells (HUV-EC-C), colon cancer cells (HT-29) and lung cancer cells (A549). However, colorectal adenocarcinoma cells (DLD-1), breast cancer cells (MCF-7) and lymphoma cells (Raji) showed higher expression of type II than that of type I Fp. Type I Fp seems to be essential for the ordinary function of complex II because

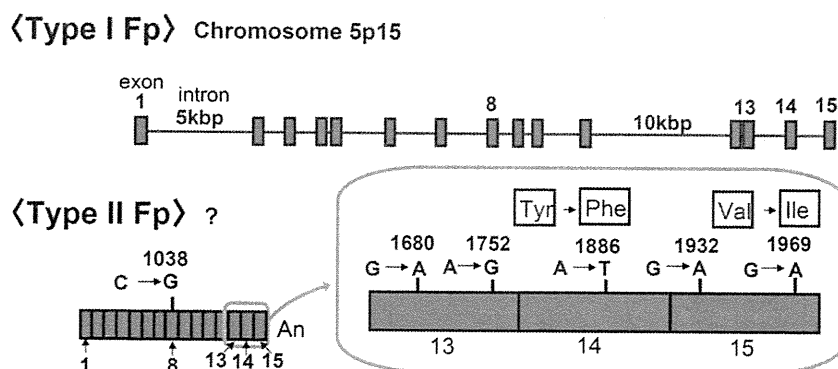**Fig. 8.** Fp isoform gene structure.Type I and II Fps differ from each other in six bases in DNA sequences and in two amino acid residues in proteins. Type I Fp gene has an exon–intron structure, while type II Fp gene issuggested to be intron-less. Although type I Fp gene is located on chromosome 5p15, the type II Fp gene is not found in the NCBI database and the location has not been clarified yet [59,60].

Human type I Fp 578 HWRKHTLSYVDVGTGKVTLEYRPVI DKTLNEADCATVPPAI RSY
Human type II Fp 578 HWRKHTLSFVDVGTGKVTLEYRPVI DKTLNEADCATIPPAI RSY
Rat Fp 570 HWRKHTLSYVDTKTGKVTLDYRPVI DKTLNEADCATVPPAI RSY
Mouse Fp 578 HWRKHTLSYVDI KTGKVTLEYRPVI DKTLNEADCATVPPAI RSY
Bovine Fp 582 HWRKHTLSYVDI KTGKVTLEYRPVI DRTLNETDCATVPPAI GSY
　　　　　　　　　　Y586F　　　　　　　　　　　　V614I

Fig. 9. Alignment of amino acid sequences of Mammalian Fp subunits.Two amino acid residues in the red box are different in human Fp isoforms. Tyr 586 and Val 614 in type I Fp are changed to Phe 586 and Ile 614 in type II Fp, respectively. Tyr 586 and Val 614 are well conserved among mammals and no animals but humans have type II Fp [59].

all the examined tissues and many of the cultured cells showed abundant expression of type I Fp and optimum pH for this isoform is around physiological mitochondrial matrix pH (pH8.0).

Since type II Fp was expressed in some cancer cells, this isoform may play an important role in the metabolism of tumor tissue. To investigate the link between type II Fp and tumor tissue in detail, we analyzed mRNA expression ratio of Fp isoforms in several tissues including tumor tissues and cultured cells. Since some tumor marker genes are expressed in fetal tissues, we included the fetal tissues in this analysis.

As shown in Table 1, in cultured cells, all the normal cells tested showed mainly type I Fp expression as reported previously [59,60]. In tissues, expression of type I Fp was higher than that of type II Fp in all the organs tested including normal testes tissue. Interestingly, normal pancreatic tissue showed higher expression of type II Fp. In addition, several tumor tissues expressed predominantly type II Fp such as breast tumor, liver tumor, kidney tumor and cervix tumor. Among fetal tissues, brain and skeletal muscle showed higher expression of type II Fp than type I Fp.

4.4. Fumarate respiration of human cancer cells

Several observations suggested the presence of a reverse reaction of complex II, fumarate reductase (FRD), in mammalian cells, although no direct evidence of FRD activity in mammalian complex II has been available until recently [62,63]. The accumulation of succinate under hypoxic conditions has been reported, and complex II has been suggested to function as FRD in mammalian cells [64]. Metabolome analysis of the cancer cells supports this idea, because succinate, fumarate and malate were present at higher levels in cancer tissues than normal tissues [65]. FRD inhibitor pyrvinium pamoate, an anthelmintic, has also been reported to act as an anticancer compound in human cancer cells [62]. Furthermore, recent biochemical studies showed fumarate respiration in human mitochondria clearly [7,8]. Mitochondria isolated from DLD-1 cells showed FRD activity with 3 nmol/min/mg protein, although this number is quite lower than that of the A. suum mitochondria (200 nmol/min/mg). Interestingly, the cancer cells had higher FRD/SQR ratio than the normal cells. For example, FRD/SQR ratio in Panc-1 cells is 0.066 ± 0.010, while that in Human Dermal Fibroblast cells is 0.011 ± 0.002. In addition, FRD/SQR ratio increased when the cancer cells were cultured under hypoxic and glucose limited condition [7]. Effect of a treatment by phosphatase and protein kinase on the direction of enzyme activity of human complex II suggests the changes from SQR to QFR by phosphorylation of Fp.

Different from A. suum, which has at least two distinct complex IIs as mentioned previously, only one gene is found for each subunit of human complex II except Fp. In this connection, it is of interest to speculate that complex II with type II Fp has higher QFR activity and plays an important role in fumarate respiration in human mitochondria as terminal oxidase of the system. Further biochemical study on
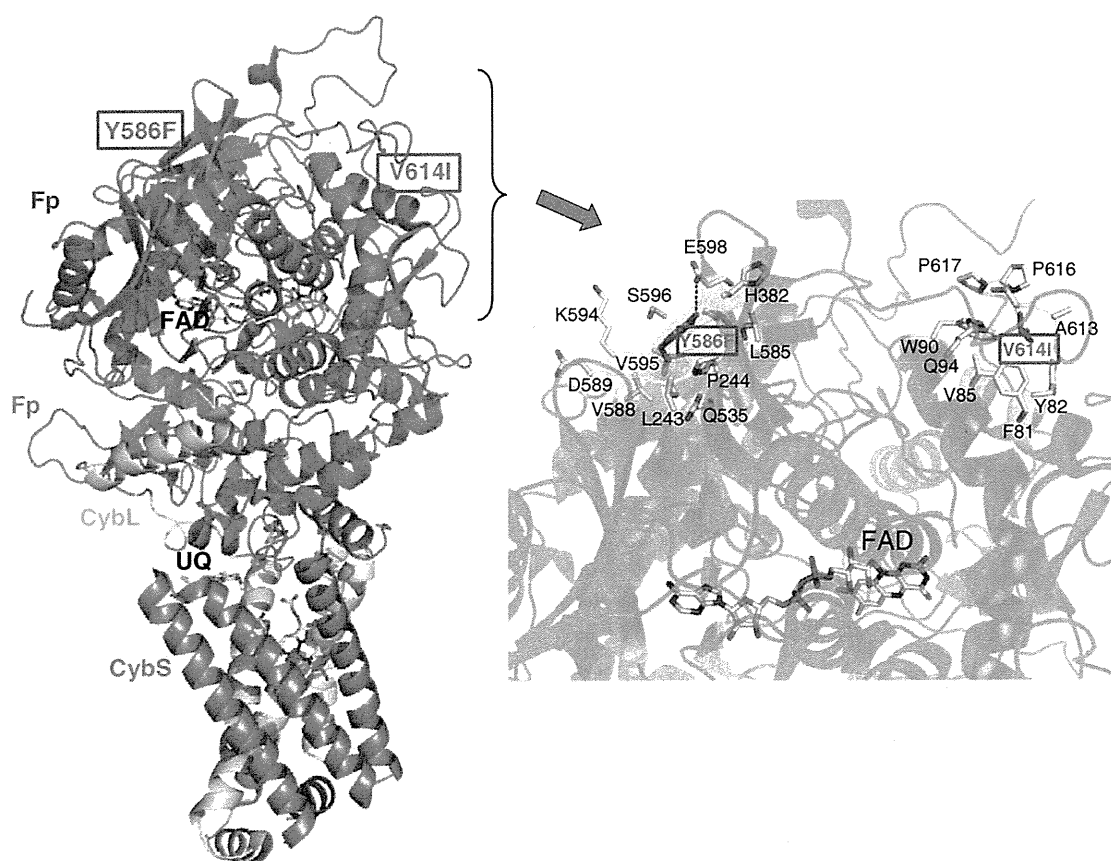

Fig. 10. Positions of Tyr 586 and Val 614 in the structure of porcine complex II.Two amino acid residues different in human isoforms, Y586F and V614I, shown in the cartoon representation of the porcine complex II structure (left) and the close-up view of the region including Y586F and V614I (right). V614I is surrounded mainly by hydrophobic residues, whereas Y586F by both hydrophilic and hydrophobic residues. Y586 and E598 are in the hydrogen bond distance (3.15 Å) to each other. UQ shows ubiquinone. The numbers of amino acid residues in the box represent the human amino acid sequences and the others are the porcine amino acid sequences.

Table 1
mRNA expression of Fp isoforms in human cultured cells and tissues.

The expression ratio of the two Fp isoforms was analyzed by RT-PCR-RFLP (restriction fragment length polymorphism with AvaII). Total RNAs were obtained from NIPPON GENE (Japan) for normal liver, heart, skeletal muscle, brain, kidney and breast tumor, colon tumor, stomach tumor and uterus tumor. Wako (Japan) for normal pancreas and fetal tissues. Invitrogen (USA) for normal testes and breast tumor, liver tumor, kidney tumor, colon tumor, pancreas tumor, cervix tumor, ovary tumor, prostate tumor. Cells; Fibroblast and Myoblast: kind gift from Dr. Yu-ichi Goto (National Institute of Neuroscience, Japan) A549, DLD-1 and MCF-7: kind gift from Mr. Yasuyuki Yamazaki (Taiho pharma ceutical, Japan) Panc-1: kind gift from Dr. Yasuhiro Esumi (National Cancer Institute, Japan) Raji: kind gift from Dr. Kazurou Shiomi (Kitasato university, Japan) HT-29, HU-VEC-C, MDA-M-231, BT-20 and T-47D: ATCC (USA). Pancreatic epithelial and stromal cells: DS pharma (Japan).

		Race	Gender	Age	I (%)/II (%)
Tissue (normal)	Liver*	Caucasoid	Female	15	70/30
	Heart*	Caucasoid	Pool of 7 donors		61/39
	Skeletal muscle*	--	Male	23	80/20
	Brain*	Caucasoid	Male	50	84/16
	Kidney*	Caucasoid	Pool of 8 donors		62/38
	Pancreas	--	Male	44	30/70
	Testes	Caucasoid	Male	19	100/0
Cell (normal)	Fibroblast*	Mongoloid	--	--	94/6
	Myoblast*	Mongoloid	--	--	87/13
	HUV-EC-C*	--	--	--	88/12
	Pancreatic epithelial	--	--	--	100/0
	Pancreatic stromal	--	--	--	100/0
Tissue (fetal)	Brain	--	Female	22 weeks	100/0
	Brain	--	Male	41 weeks	38/62
	Skeletal muscle	--	Male	22 weeks	0/100
	Skeletal muscle	--	Female	19 weeks	100/0
Tissue (cancer)	Breast	--	Female	55	100/0
	Breast	Mongoloid	Female	Pool of 6 donors	0/100
	Liver	Caucasoid	Male	60	0/100
	Kidney	Caucasioid	Female	54	23/77
	Colon	Caucasoid	Male	75	100/0
	Colon	--	--	--	100/0
	Pancreas	Mongoloid	Male	32	100/0
	Stomach	--	--	--	100/0
	Uterus	--	Female	--	100/0
	Cervix	Caucasoid	Female	59	23/77
	Ovary	Caucasoid	Female	32	100/0
	Prostate	--	Male	--	100/0
Cell (cancer)	HT29*	Caucasoid	Female	44	92/8
	A549*	Caucasoid	Male	58	96/4
	DLD-1*	--	Male	--	25/75
	MCF-7*	Caucasoid	Female	69	23/77
	Raji*	Neglod	Male	11	17/83
	Panc-1	Caucasoid	Male	56	12/88
	MDA-M-231	Caucasoid	Female	51	100/0
	BT-20	Caucasoid	Female	78	78/22
	T-47D	Caucasoid	Female	54	53/47

* Tomitsuka, et al. [59,60].

the difference between type I and type II Fp will bring final conclusion on this attractive idea.

5. Conclusions

The recent findings described in this review indicate that the respiratory chain plays an important role in responses to changes in the amount of oxygen in the environment. Complex II functions as a fumarate reductase during adaptation to a hypoxic condition to ensure the maintenance of oxygen homeostasis. In this connection, the reports indicating that complex II functions as an oxygen sensor are of great interest [63].

In addition, direct evidence of fumarate respiration in human mitochondria are quite important in the study of energy metabolism in hypoxic condition including cancer cells. Differences in energy metabolism between hosts and parasites and/or cancer cells are attractive therapeutic targets.

References

[1] K. Kita, K. Shiomi, S. Ōmura, Parasitology in Japan: advances in drug discovery and biochemical studies, Trends Parasitol. 23 (2007) 223–229.
[2] A. Kroger, V. Geisler, E. Lemma, F. Theis, R. Lenger, Bacterial fumarate respiration, Arch. Microbiol. 158 (1992) 311–314.
[3] T. Kuramochi, H. Hirawake, S. Kojima, S. Takamiya, R. Furushima, T. Aoki, R. Komuniecki, K. Kita, Sequence comparison between the flavoprotein subunit of the fumarate reductase (complex II) of the anaerobic parasitic nematode, Ascaris suum and the succinate dehydrogenase of theaerobic, free-living nematode, Caenorhabditis elegans, Mol. Biochem. Parasitol. 68 (1994) 177–187.
[4] F. Saruta, H. Hirawake, S. Takamiya, Y.-C. Ma, T. Aoki, K. Sekimizu, S. Kojima, K. Kita, Cloning of a cDNA encoding the small subunit of cytochrome b_{558} (cybS) of mitochondrial fumarate reductase (complex II) from adult Ascaris suum, Biochim. Biophys. Acta 1276 (1996) 1–5.
[5] H. Amino, H. Wang, H. Hirawake, F. Saruta, D. Mizuchi, R. Mineki, N. Shindo, K. Murayama, S. Takamiya, T. Aoki, S. Kojima, K. Kita, Stage-specific isoforms of Ascaris suum complex II: the fumarate reductase of the parasitic adult and the succinate dehydrogenase of free-living larvae share a common iron-sulfur subunit, Mol. Biochem. Parasitol. 106 (2000) 63–76.
[6] K. Kita, S. Takamiya, Electron-transfer complexes in Ascaris mitochondria, Adv. Parasitol. 51 (2002) 95–131.
[7] E. Tomitsuka, K. Kita, H. Esumi, Regulation of succinate–ubiquinone reductase and fumarate reductase activities in human complex II by phosphorylation of its flavoprotein subunit, Proc. Jpn. Acad. Ser. B Phys. Biol. Sci. 85 (2009) 258–265.
[8] E. Tomitsuka, K. Kita, H. Esumi, The NADH-fumarate reductase system, a novel mitochondrial energy metabolism, is a new target for anticancer therapy in tumor microenvironments, Ann. N. Y. Acad. Sci. 201 (2011) 44–49.
[9] M.P. Paranagama, K. Sakamoto, H. Amino, M. Awano, H. Miyoshi, K. Kita, Contribution of the FAD and quinone binding sites to the production of reactive oxygen species from Ascaris suum mitochondrial complex II, Mitochondrion 10 (2010) 158–165.
[10] R.D. Guzy, B. Sharma, E. Bell, N.S. Chandel, P.T. Schumacker, Loss of the SdhB, but Not the SdhA, subunit of complex II triggers reactive oxygen species-dependent hypoxia-inducible factor activation and tumorigenesis, Mol. Cell. Biol. 28 (2008) 718–731.
[11] M.A. Selak, S.M. MacKenzie, H. Boulahbel, D.G. Watson, K.D. Mansfield, Y. Pan, M.C. Simon, C.B. Thompson, E. Gottlieb, Succinate links TCA cycle dysfunction to oncogenesis by inhibiting HIF-alpha prolyl hydroxylase, Cancer Cell 7 (2005) 77–85.
[12] R. Komuniecki, B.G. Harris, J. Marr, M. Mueller, Biochemistry and Molecular Biology of Parasites, Academic Press, London, 1995, pp. 49–66.
[13] A.G.M. Tielens, J. Van Hellemond, The electron transport chain in anaerobically functioning eukaryotes, Biochim. Biophys. Acta 1365 (1998) 71–78.
[14] K. Kita, H. Hirawake, S. Takamiya, Cytochromes in the respiratory chain of helminth mitochondria, Int. J. Parasitol. 27 (1997) 617–630.
[15] J. Matsumoto, K. Sakamoto, N. Shinjyo, Y. Kido, N. Yamamoto, K. Yagi, H. Miyoshi, N. Nonaka, K. Katakura, K. Kita, Y. Oku, Anaerobic NADH-fumarate reductase system is predominant in the respiratory chain of Echinococcus multilocularis, providing a novel target for the chemotherapy of alveolar echinococcosis, Antimicrob. Agents Chemother. 52 (2008) 164–170.
[16] P. Kohler, R. Bachmann, Mechanisms of respiration and phosphorylation in Ascaris muscle mitochondria, Mol. Biochem. Parasitol. 1 (1980) 75–90.
[17] H. Oya, K. Kita, in: E. Bennet, C. Behm, C. Bryant (Eds.), Comparative Biochemistry of Parasitic Helminths, Chapman and Hall, London, 1988, pp. 35–53.
[18] S. Takamiya, R. Furushima, R.H. Oya, Electron transfer complexes of Ascaris suum muscle mitochondria: I. Characterization of NADH-cytochrome c reductase (complex I–III), with special reference to cytochrome localization, Mol. Biochem. Parasitol. 13 (1984) 121–134.
[19] S. Takamiya, K. Kita, H. Wang, P.P. Weinstein, A. Hiraishi, H. Oya, T. Aoki Developmental, Changes in the respiratory chain of Ascaris mitochondria, Biochim. Biophys. Acta 1141 (1993) 65–74.
[20] S.T. Cole, C. Condon, B.D. Lemire, J.H. Weiner, Molecular biology, biochemistry and bioenergetics of fumarate reductase, a complex membrane-bound iron–sulfur flavoenzyme of Escherichia coli, Biochim. Biophys. Acta 811 (1985) 381–403.
[21] A. Hiraishi, Fumarate reduction systems in members of the family Rhodospirillaceae with different quinone types, Arch. Microbiol. 150 (1988) 56–60.
[22] F. Iwata, N. Shinjyo, H. Amino, K. Sakamoto, M.K. Islam, N. Tsuji, K. Kita, Change of subunit composition of mitochondrial complex II (succinate-ubiquinone reductase/quinol-fumarate reductase) in Ascaris suum during the migration in the experimental host, Parasitol. Int. 57 (2008) 54–61.